Diabetologia (2004) 47:638–647
DOI 10.1007/s00125-004-1366-y

Diabetologia

Genes for systemic vascular complications are differentially expressed in the livers of Type 2 diabetic patients

T. Takamura[1] · M. Sakurai[1] · T. Ota[1] · H. Ando[1] · M. Honda[1] · S. Kaneko[1]

[1] Department of Diabetes and Digestive Disease, Kanazawa University Graduate School of Medical Science, Kanazawa, Japan

Abstract

Aims/hypothesis. Type 2 diabetes is characterised by excessive hepatic glucose production and frequently leads to systemic vascular complications. We therefore analysed the relationship between the gene expression profile in the liver and the pathophysiology of Type 2 diabetes.

Methods. Liver biopsy samples were obtained from twelve patients with Type 2 diabetes and from nine non-diabetic patients. To assay gene expression globally in the livers of both groups, we made complementary DNA (cDNA) microarrays consisting of 1080 human cDNAs. Relative expression ratios of individual genes were obtained by comparing cyanine 5-labelled cDNA from the patients with cyanine 3-labelled cDNA from reference RNA from the liver of a non-diabetic patient.

Results. On assessing the similarities of differentially expressed genes, the gene expression profiles of the twelve diabetic patients formed a separate cluster from those of the non-diabetic patients. Of the 1080 genes assayed, 105 (9.7%) were up-regulated and 134 (12%) were down-regulated in the diabetic livers ($p<0.005$). The genes up-regulated in the diabetic patients included those encoding angiogenic factors such as vascular endothelial growth factor, endothelin and platelet-derived growth factor. They also included TGF superfamily genes such as *TGFA* and *TGFB1* as well as bone morphogenetic proteins. Among the down-regulated genes in the diabetic patients were molecules defending against stress, e.g. flavin-containing monooxygenase and superoxide dismutase.

Conclusions/interpretation. These findings suggest that livers of patients with Type 2 diabetes have gene expression profiles indicative of an increased risk of systemic vascular complications.

Keywords cDNA microarray · Liver · Type 2 diabetes · Vascular complications

Received: 14 October 2003 / Accepted: 19 January 2004
Published online: 26 March 2004

S. Kaneko (✉)
Department of Diabetes and Digestive Disease,
Kanazawa University Graduate School of Medical Science,
Kanazawa, Japan
E-mail: skaneko@medf.m.kanazawa-u.ac.jp
Tel.: +81-76-265-2243, Fax: +81-76-234-4250

Abbreviations: aRNA, antisense RNA · BMP, bone morphogenetic protein · cDNA, complementary DNA · Cy, cyanine · FMO, flavin-containing monooxygenase · NASH, non-alcoholic steatohepatitis · PDGF, platelet-derived growth factor · SSC, standard saline citrate · SOD, superoxide dismutase · VCAM, vascular cell adhesion molecule · VEGF, vascular endothelial growth factor

Electronic Supplementary Material
Supplementary material is available in the online version of this article at http://dx.doi.org/10.1007/s00125-004-1366-y

Introduction

Type 2 diabetes, the most common form of diabetes mellitus, results from the interaction of genetic and environmental factors. Although a few cases of Type 2 diabetes involve monogenic syndrome, in which the onset of disease in young patients is predictable, the majority of cases involve multiple genetic alterations [1]. The liver plays a central role in glucose homeostasis, and Type 2 diabetes is characterised by excessive hepatic glucose production. Due to its long duration, the disease causes systemic vascular complications such as micro- and macroangiopathy. Indeed, the liver is also a major source of angiogenic factors and cytokines involved in the development of atherosclerosis, e.g. vascular endothelial growth factor (VEGF) and TGF [2, 3]. For this reason, a comprehensive analysis of gene expression in the liver could deepen understanding of Type 2 diabetes and its related complications.

The recently developed complementary DNA (cDNA) microarray technology allows simultaneous, parallel analysis of the expression of hundreds to thousands of genes in cell lines or tissues, as well as the investigation of drug-induced changes in gene expression [4]. We have already used cDNA microarrays, consisting of 1080 human cDNAs, to characterise alterations that occur in various liver diseases [5, 6]. More recently, microarray profiling of skeletal muscle tissue of Type 2 diabetic patients [7, 8] and of healthy humans treated with insulin [9] has been reported. Although the liver is central for glucose homeostasis, microarray profiling of diabetic liver has been done only in Ob/Ob mice, a genetically obese rodent model of diabetes [10, 11, 12]. We have now used it to clarify the transcriptional alterations in the liver that are associated with the pathophysiology of Type 2 diabetes. We have also used this methodology to determine differentially expressed liver genes that are representative of increased risk for systemic diabetic vascular complications.

Subjects and methods

Patients. The subjects were twelve patients with Type 2 diabetes and nine non-diabetic patients serially recruited between 1998 and 2001 at Kanazawa University Hospital, Japan. There were no significant differences in age, BMI and liver function tests between diabetic and non diabetic patients (Table 1). Informed consent was obtained from all subjects, and the experimental protocol was approved by our institution.

All subjects tested negative for hepatitis B and C viruses. The diabetic patients were diagnosed according to criteria established by an expert committee on the diagnosis and classification of diabetes mellitus [1]. The diabetic patients (DM 1 to DM 12) were treated either with diet therapy alone (DM 7, 10 and 11), or with an α-glucosidase inhibitor (DM 6 and 8) or with insulin (DM 1 to 5, 9 and 12). None of them was taking any other oral hypoglycaemic agent. Pharmacological treatments other than anti-diabetic treatments included diltiazem hydrochloride (DM 3), nicorandil (DM 6) and nifedipine (DM 6) for angina pectoris. No statins, angiotensin-converting enzyme inhibitors or angiotensin II receptor blockers were being taken.

Table 1. Characteristics of subjects

Characteristic	Type 2 diabetic patients	Non-diabetic patients
Men/women	11/1	5/4
Age (years)	47±11	55±11
BMI (kg/m^2)	28±4	25±3
FPG (μmol/l)	6.7±1.7*	5.3±0.6
HbA_1c (%)	7.1±1.5*	5.0±0.6
AST (IU/l)	40±25	27±13
ALT (IU/l)	55±38	29±14
HOMA-R	4.14±2.45	ND

Data are expressed as means ± SD. FPG, fasting plasma glucose; AST, aspartate transaminase; ALT, alanine aminotransferase; HOMA-R, homeostasis model insulin resistance index; ND, not determined. *$p<0.05$ vs non-diabetic patients

Informed consent was obtained from the diabetic patients both for this study and for the histolological examination of liver diseases, including non-alcoholic steatohepatitis (NASH), which is often associated with diabetes [13]. Liver biopsy specimens were obtained from all diabetic patients, immediately frozen in liquid nitrogen and stored at –80 °C until use. The nine non-diabetic subjects (Non-DM 1 to 9) were patients undergoing resection for colon cancer; for each, a tissue specimen was surgically removed from the non-cancerous part of the liver. The non-diabetic subjects were not taking medication, except anti-indigestion or anti-ulcer agents. Informed consent was also obtained from them for this study.

The study was approved by the relevant ethics committee and was carried out in accordance with the Declaration of Helsinki.

Pathology of the liver. All liver biopsy specimens were examined using haematoxylin-eosin and silver reticulin stain. A pathologist who was blinded to the patients' clinical condition and biochemical data scored each biopsy for steatosis, inflammation and fibrosis, using previously reported criteria [14, 15]. Steatosis was scored as 0 (no steatosis), 1 (in less than 5% of the lobular parenchyma), 2 (in 5–25% of the lobular parenchyma), 3 (in 25–75% of the lobular parenchyma) or 4 (in more than 75% of the lobular parenchyma). Inflammation was scored as 0 (no hepatocyte injury or inflammation), 1 (sparse injury and/or inflammation), 2 (mild focal injury and/or inflammation), 3 (noticeable injury and/or inflammation) or 4 (severe zone 3 hepatocyte injury and/or inflammation). Fibrosis was scored as 0 (normal connective tissue), 1 (focal pericellular fibrosis in zone 3), 2 (perivenular and pericellular fibrosis confined to zones 2 and 3 with or without portal and/or periportal fibrosis), 3 (bridging or extensive fibrosis with architectural distortion) or 4 (cirrhosis). No subjects had severely inflamed or fibrotic livers (score of 3 or higher).

Preparation of cDNA microarray slides. The protocol for preparing microarray slides containing 1080 cDNA clones has been described [5, 6]. The genes to be spotted were selected from the Clontech atlas membrane array and obtained from IMAGE Consortium libraries through its distributor, Research Genetics (Huntsville, Ala., USA). Each sequence-

verified clone was repeatedly sequenced in our laboratory to avoid using cross-contaminated clones. Sequence homology was confirmed using the advanced BLAST search program (http://www.ncbi.nlm.nih.gov/BLAST/). When sequencing failed to verify the purity of IMAGE clones for key genes, corresponding clones were obtained from RIKEN Gene Bank (Takaodai, Tukuba, Japan) or through personal communication. Of the 1080 cDNA clones used for analysis, 1001 were sequence-verified and 79 were sequence-unverified human expressed sequence tag clones. As negative controls for each assay, we used Firefly luciferase (Promega, Madison, Wis., USA) sequences, which have no homology to sequences in the human genome. Polymerase chain reaction products prepared from these clones were spotted on to glass slides with 16 pins using SPBIO 2000 (Hitachi Software, Fukuoka, Japan). To normalise varying efficiencies of labelling and detection, a series of housekeeping genes (encoding β-actin, ribosomal protein L32, GAPDH and albumin), as well as firefly luciferase sequences, were spotted in each of the 16 rectangles of DNA spots.

RNA isolation and antisense RNA amplification. Total RNA was isolated from frozen liver tissue samples using an RNA extraction kit [5], and first-strand cDNA was synthesised with Superscript II reverse transcriptase (GIBCO-BRL, Gaithersburg, Md., USA). Second-strand cDNA was synthesised with *Escherichia coli* DNA ligase and *E. coli* DNA polymerase (both from New England Biolabs, Beverly, Mass., USA) as described [5], and double-stranded cDNA was purified by phase lock gel (Eppendorf, Westbury, N.Y., USA) with phenol/chloroform extraction. We subsequently used double-stranded cDNA as a template for in vitro antisense RNA (aRNA) transcription and amplification using a MEGA script T7 kit (Ambion, Austin, Tex., USA) according to the manufacturer's protocol. The resulting aRNA was purified on an affinity resin column (RNeasy Mini Kit, Qiagen, Chatsworth, Calif., USA). All aRNAs were stored at −80 °C until use.

Preparation of fluorescence-labelled cDNA and microarray hybridisation. To label the probes, approximately 2 to 3 μg of aRNA was used as a template for first-strand cDNA synthesis with cyanine (Cy) 3- or Cy5-deoxyuridine triphosphate (Amersham Biosciences, Piscataway, N.J., USA) and Superscript II reverse transcriptase [5]. As a reference for each microarray analysis, we used aRNA samples prepared from the normal liver tissue of a 72-year-old man with a single liver tumour. Reference aRNAs were labelled with Cy3 and test sample aRNAs with Cy5. The labelled probes were purified on Microcon 30 columns (Millipore, Bedford, Mass., USA), and then the blocking reagents 10 μg yeast transfer RNA, 4 μg poly(dA) and 15 μg human Cot DNA were added to each probe and each mixture was concentrated to 12 μl. We then added 2.55 μl 20× standard saline citrate (SSC) and 0.45 μl 10% sodium dodecyl sulfate to each mixture, and each 15 μl aliquot was used as a hybridisation probe for each cDNA-spotted slide. The slides were covered with glass coverslips and fixed in a hybridisation cassette (TeleChem, Sunnyvale, Calif., USA), then hybridisation was performed for 12 hours at 65 °C. Slides were washed in 2× SSC and 0.03% sodium dodecyl sulfate, in 1× SSC and in 0.2× SSC; each washing lasted 5 minutes.

Image analysis. Quantitative assessment of the signals on the slides was done by scanning on a ScanArray 5000 (General Scanning, Watertown, Mass., USA), followed by image analysis using ImaGene 3.0 software (Bio Discovery, Los Angeles, Calif., USA). The signal intensity of each spot was corrected by subtracting adjacent background signals. To normalise the data, we averaged the intensities of all spots obtained with Cy3 and Cy5 in each of the 16 rectangles and adjusted the intensity of each corrected DNA spot by the average intensity ratio of Cy5:Cy3 (=1.0). This global normalisation of intensity provided a smaller variance of the Cy5:Cy3 ratio and almost the same results as normalisation using the housekeeping genes. Because signal values of approximately 500 to 600 were obtained for luciferase genes, which have no homology to any human gene sequence, all values below 600 were set as background values.

Hierarchical clustering of the gene expression of the patients was assessed by calculating Pearson's product–moment correlation coefficient using the program Cluster, and by visualisation using 'Tree View' (http://genexpress.stanford.edu). The data were log-transferred, normalised, mean-centred and applied to the average linkage clustering. The resulting dendrogram indicated the order in which patients were grouped according to similarities in their gene expression patterns. The gene cluster data were presented graphically as coloured images, and the genes that had been analysed were arranged as ordered by the clustering algorithm, so that genes with the most similar expression patterns were adjacent to each other.

Real-time quantitative PCR. Double-strand cDNA was used as a template for real-time quantitative PCR of bone morphogenetic protein-4 (*BMP4*), *TGFB1*, endothelin and glutathione S-transferase theta 1. To do this we used the ABI Prism 7700 Sequence Detection System (Applied Biosystems, Foster City, Calif., USA). The sets of primers and TaqMan probes were proprietary to Applied Biosystems (Assays-on-Demand gene expression product). To control for variation in the amount of DNA available for PCR in the different samples, gene expression of the target sequence was normalised relative to expression of an endogenous control, 18S ribosomal RNA (18S rRNA TaqMan Control Reagent Kit, Applied Biosystems). The PCR conditions were 1 cycle at 50 °C for 2 min and at 95 °C for 10 min, followed by 40 cycles at 95 °C for 15 s and at 60 °C for 1 min.

Statistical analysis. All data are expressed as means ± SEM. To test the significance of numbers and frequencies of genes or Cy5:Cy3 ratios, we used supervised analyses with the permutation-based method (BRB-ArrayTools, http://linus.nci.nih.gov/BRB-ArrayTools.html) [16]. This software for the statistical analysis of cDNA microarray gene expression data was developed by the Biometric Research Branch of the National Cancer Institute (USA). It contains a class comparison tool based on univariate F tests to find genes differentially expressed between predefined clinical groups. The permutation distribution of the F statistic, based on 2000 random permutations, was also used to confirm statistical significance. A p value of less than 0.005 was considered significant.

Results

Histological findings in the livers of Type 2 diabetic patients. The clinical characteristics of the diabetic and non-diabetic patients were similar, except for diabetic markers (Table 1). Histological examination of the livers of Type 2 diabetic patients revealed various degrees of steatosis, inflammation and fibrosis (Table 2), although all had normal liver function (Table 1). We did not identify any patients with advanced NASH, or whose livers revealed severe inflammation or fibrosis

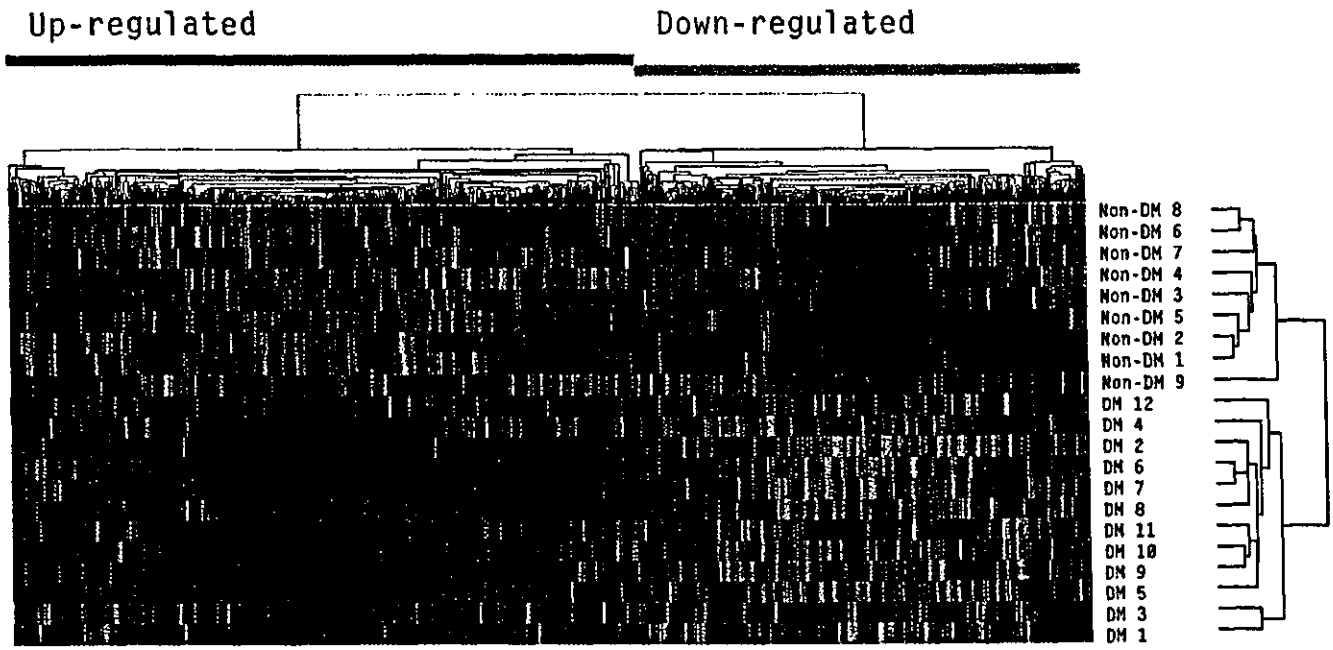

Fig. 1. Hierarchical clustering analysis of gene expression profiles in the livers of twelve diabetic and nine non-diabetic patients. Genes up-regulated in diabetic livers are shown in red; genes down-regulated in diabetic livers are in green. DM, Type 2 diabetic patient; Non-DM, non-diabetic patient

Table 2. Histological scoring of steatosis, inflammation and fibrosis in the livers of non-diabetic and Type 2 diabetic patients

	Steatosis	Inflammation	Fibrosis		Steatosis	Inflammation	Fibrosis
Non-DM 1	0	0	0	DM 1	3	2	2
Non-DM 2	0	0	0	DM 2	1	0	2
Non-DM 3	0	0	0	DM 3	1	1	1
Non-DM 4	0	0	0	DM 4	1	1	1
Non-DM 5	0	0	0	DM 5	3	2	2
Non-DM 6	0	0	0	DM 6	1	1	1
Non-DM 7	0	0	0	DM 7	2	1	1
Non-DM 8	0	0	0	DM 8	3	2	0
Non-DM 9	0	0	0	DM 9	2	0	2
				DM 10	1	0	0
				DM 11	4	1	1
				DM 12	2	1	1
Mean	0.0	0.0	0.0	Mean	2.0	1.0	1.2
SD	0.0	0.0	0.0	SD	1.0	0.7	0.7

Scoring was on a scale of 0 to 4. Non-DM, liver of non-diabetic patient; DM, liver of Type 2 diabetic patient

(score of 3 or more). The livers of all non-diabetic patients were histologically normal (Table 2).

Hierarchical clustering of gene expression. Hierarchical clustering of gene expression in the livers of all 21 patients was assessed by calculating Pearson's product–moment correlation coefficient (Fig. 1). For differentially expressed genes, the patients clustered into two groups, with one cluster being the twelve diabetic patients and the second cluster being the nine non-diabetic patients. The presence of diabetes was the only clinical determinant of gene expression contributing to clustering. In contrast, age, sex and BMI were not clinical determinants of gene expression profiling (data not shown). Differences in the clustering of diabetic and non-diabetic patients was observed using three subsets of genes: (i) transcription factors (95 genes); (ii) cytokines and growth factors (154 genes); and (iii) apoptosis-related genes (114 genes) (data not shown). These results suggest that the livers of diabetic patients have different patterns of gene expression than livers of non-diabetic persons.

Identification of differentially expressed genes in the livers of Type 2 diabetic patients. In characterising the differentially expressed genes in the livers of patients with Type 2 diabetes, we found that of the 1080 sequences assayed 105 (9.7%) were significantly up-

Table 3. Representative genes significantly up-regulated in the livers of Type 2 diabetic patients

GenBank Ref. Seq. ID	Gene	DM/ Non-DM	Parametric *p* value
Signal transduction			
NM_002747	Mitogen-activated protein kinase 4 (MAPK4; p63)	1.36	0.0000001
NM_000924	Calmodulin-dependent phosphodiesterase PDE1B1	1.81	0.0000017
NM_005512	Garp gene	1.56	0.0000036
NM_000835	Glutamate receptor, ionotropic, *N*-methyl D-aspartate 2C	1.32	0.0001347
NM_000675	Adenosine receptor	1.60	0.0001912
NM_004878	Homo sapiens Pig12 (PIG12)	1.39	0.0003145
NM_130850	Bone morphogenetic protein 4	1.38	0.0003244
NM_002045	Growth-associated protein 43	1.67	0.0005587
NM_001719	Bone morphogenetic protein 7 (osteogenic protein 1)	1.45	0.0006087
NM_145751	TRAF2	1.40	0.0008602
NM_145803	TNF receptor-associated factor 6	1.59	0.0015876
NM_024408	Notch 2	1.52	0.0033336
Cell adhesion/cell–cell signal			
NM_004932	Cadherin 6, K-cadherin (fetal kidney)	1.45	0.0000026
NM_001850	Collagen, type VIII, alpha 1	1.50	0.0000038
NM_002206	Integrin, alpha 7	1.32	0.0000111
NM_000887	Integrin, alpha X (antigen CD11C [p150], alpha polypeptide)	1.30	0.0000127
NM_002286	Lymphocyte-activation gene 3	1.22	0.0000212
NM_005562	Nicein B2 chain	1.36	0.0000351
NM_005562	Integrin, beta 7	1.38	0.0000532
NM_032966	Burkitt lymphoma receptor 1, GTP-binding protein	1.28	0.0000604
NM_002658	Plasminogen activator, urokinase	1.40	0.0001332
NM_001264	Corneodesmosin	1.47	0.0002728
NM_080679	Collagen, type XI, alpha 2	1.49	0.0002958
NM_033641	Collagen, type IV, alpha 6	1.25	0.0004334
NM_004061	Cadherin 12 (*N*-cadherin 2)	1.37	0.0004492
NM_002214	Integrin, beta 8	1.28	0.0012977
NM_002428	Matrix metalloproteinase 15 (membrane-inserted)	1.26	0.0029267
Cytokine/growth factor-related			
NM_001956	Endothelin 2	1.56	0.0000030
NM_000575	Interleukin 1, alpha	1.68	0.0000069
NM_002009	Fibroblast growth factor 7 (keratinocyte growth factor)	1.87	0.0000080
NM_003236	Transforming growth factor, alpha	1.52	0.0000319
NM_005429	Vascular endothelial growth factor C	1.38	0.0000673
NM_000601	HGF agonist/antagonist	1.24	0.0002486
NM_002045	Growth-associated protein 43	1.67	0.0005587
NM_023105	Fibroblast growth factor receptor 1 (fms-related tyrosine kinase 2)	1.31	0.0007361
NM_033016	Platelet-derived growth factor beta	1.37	0.0007417
NM_002506	Nerve growth factor, beta polypeptide	1.26	0.0012522
NM_147187	Tumor necrosis factor receptor superfamily, member 10b	1.31	0.0012870
NM_001957	Endothelin receptor type A	1.22	0.0016449
NM_004447	Epidermal growth factor	1.25	0.0017034
NM_006207	Platelet-derived growth factor receptor-like	1.27	0.0022775
NM_003247	Thrombospondin 2	1.24	0.0045472
Transcription/translation factor			
NM_002934	Ribonuclease, RNase A family, 2 (liver, eosinophil-derived neurotoxin)	1.37	0.0000369
NM_005522	Human HOXA1	1.39	0.0001436
Stress response			
NM_007294	BRCA1	1.64	0.0000002
NM_000465	BRCA1-associated RING domain 1	1.94	0.0000078
NM_000852	Glutathione S-transferase pi	1.58	0.0000842
NM_000853	Glutathione S-transferase T1	2.84	0.0001879
NM_004134	Heat shock 70kD protein 9B (mortalin-2)	1.22	0.0002101
NM_006904	Human DNA-dependent protein kinase catalytic subunit (DNA-PKcs)	1.26	0.0006155
NM_002542	8-oxoguanine DNA glycosylase	1.24	0.0033415

Table 3. (continued)

GenBank Ref. Seq. ID	Gene	DM/ Non-DM	Parametric *p* value
Metabolism			
NM_015865	RACH1 (RACH1)	1.41	0.0000333
NM_000022	Adenosine deaminase	1.21	0.0001155
Cell cycle/apoptosis/oncogenesis			
NM_001254	CDC18 (cell division cycle 18, *S. pombe*, homolog)-like	1.44	0.0000060
NM_001168	Apoptosis inhibitor 4 (survivin)	1.86	0.0000177
NM_001786	Cell division cycle 2, G1 to S and G2 to M	1.29	0.0002815
NM_022809	Cell division cycle 25C	1.29	0.0002819
NM_005521	HOX11=HOX11 homeodomain {homeobox}	1.20	0.0005101
NM_004397	DEAD/H (Asp-Glu-Ala-Asp/His) box polypeptide 6 (RNA helicase, 54kD)	1.30	0.0006865
NM_000546	p53	1.39	0.0020913

We identified 105 genes that were up-regulated in the livers of Type 2 diabetic patients ($p<0.005$). Expressed sequence tags and genes with unknown function are not listed. DM, livers from Type 2 diabetic patients; Non-DM, livers from non-diabetic patients

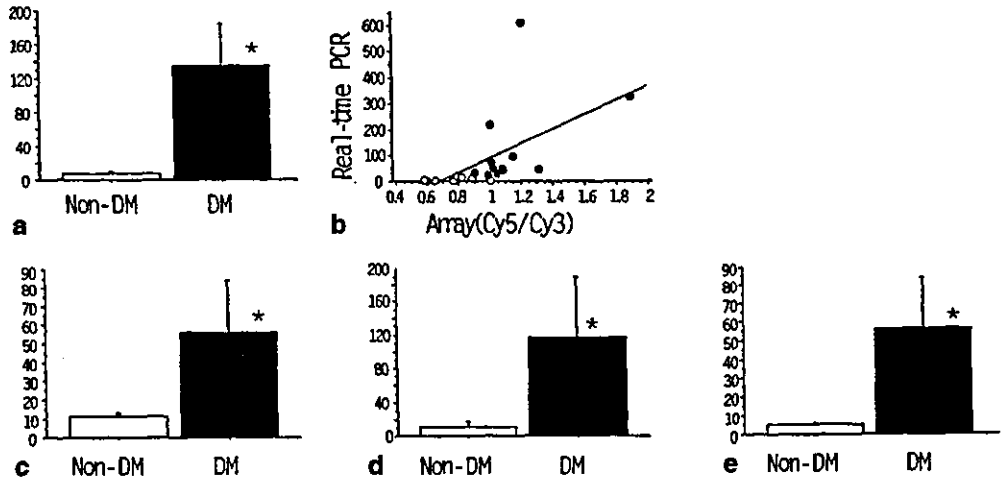

Fig. 2. Expression of gene transcripts by real-time quantitative PCR (**a–e**) and (**b**) gene expression levels assessed by cDNA microarray and real-time quantitative PCR. Double-strand complementary DNAs (cDNA) were used as templates for expression of bone morphogenetic protein 4 (*BMP4*) (**a, b**), endothelin (**c**), glutathione S-transferase theta 1 (**d**) and *TGFB1* (**e**) mRNAs. Expression of each target sequence was normalised relative to the expression of 18S ribosomal RNA. Each bar represents means ± SD. The correlation (**b**) between *BMP4* gene expression levels assessed by cDNA microarray and real-time quantitative PCR was significant ($r=0.58$, $p=0.0053$). ●, Type 2 diabetic patients; ○, non-diabetic patients. Non-DM, liver of non-diabetic patients; DM, liver of Type 2 diabetic patients; Cy, cyanine. * $p<0.05$ vs Non-DM

regulated and 134 (12%) were significantly down-regulated, compared with those of non-diabetic patients ($p<0.005$ by univariate F tests) (Tables 3 and 4). Although our cDNA microarrays did not contain many genes associated with glucose and lipid metabolism, expression of other genes was differentially altered in patients with Type 2 diabetes.

Interestingly, the genes significantly up-regulated included: (i) those encoding angiogenic factors, such as VEGF, endothelin and platelet-derived growth factor (PDGF); (ii) members of the TGF superfamily, including TGF-α and BMP-4 and –7; and (iii) collagens IV and VIII (Table 3). Also up-regulated were genes coding for pro-inflammatory cytokines or their receptors, e.g. interleukin 1 alpha, fibroblast growth factor and tumour necrosis factor receptor, and stress-response proteins, including glutathione S-transferase T1 and 8-oxoguanine DNA glycosylase (Table 3).

In contrast, the following genes were down-regulated in diabetic compared with non-diabetic livers: genes coding for general transcription factors, such as TFII and Jun; genes coding for lipogenic enzymes, including fatty acid desaturase and CD36 (fatty acid translocase); and genes coding for the ketogenic enzyme, acetoacetyl coenzyme A thiolase (Table 4). Also down-regulated in the livers of diabetic patients were genes encoding cell–cell interaction molecules, such as fibronectin, vascular cell adhesion molecule (VCAM)-1, selectin L, ficolin, decorin and MHC classes I and II, as well as stress defence molecules

Table 4. Representative genes significantly down-regulated in the livers of Type 2 diabetic patients

GenBank Ref. Seq. ID	Gene	DM/ Non-DM	Parametric *p* value
Transcription/translation factor			
NM_003407	Zinc finger protein homologous to Zfp-36 in mouse	0.37	0.0000096
NM_002126	Hepatic leukaemia factor	0.49	0.0000119
NM_001514	General transcription factor IIB (TFIIB)	0.46	0.0000227
NM_002228	c-jun proto oncogene (JUN)	0.45	0.0000238
NM_002052	GATA-binding protein 4	0.57	0.0000286
NM_002568	Poly(A)-binding protein, cytoplasmic 1	0.49	0.0000295
NM_004514	Interleukin enhancer binding factor 1	0.56	0.0000567
NM_003998	Nuclear factor of kappa light polypeptide gene enhancer in B-cells 1 (p105)	0.76	0.0001071
NM_006756	TRANSCRIPTION ELONGATION FACTOR S-II	0.59	0.0001304
NM_006195	Pre-B-cell leukaemia transcription factor 3	0.69	0.0001337
NM_001806	CCAAT/enhancer binding protein (C/EBP), gamma	0.79	0.0001430
NM_139276	Signal transducer and activator of transcription 3	0.61	0.0001961
NM_134447	RPB5-mediating protein (RMP)	0.53	0.0002762
NM_139266	STAT1	0.69	0.0003492
NM_001416	eIF4A	0.51	0.0004738
NM_006565	Transcriptional repressor (CTCF)	0.76	0.0005205
NM_080648	Ref-1	0.73	0.0005552
NM_004094	eIF2A	0.69	0.0006909
NM_003750	eIF3-p170	0.49	0.0007163
NM_005194	NF-IL6	0.50	0.0016377
Cell adhesion/cell-cell signal			
NM_080682	VCAM 1	0.51	0.0000012
NM_021983	MHC class II DR beta 4	0.39	0.0000013
NM_002026	Fibronectin	0.54	0.0000055
NM_004615	Transmembrane 4 superfamily member 2	0.61	0.0000157
NM_000655	Selectin L (lymphocyte adhesion molecule 1)	0.63	0.0000192
NM_004415	Desmoplakin I and II	0.57	0.0000556
NM_004559	MHC class II, Y box-binding protein I; DNA-binding protein B	0.56	0.0002113
NM_004530	Matrix metalloproteinase 2 (gelatinase A, 72kD type IV collagenase)	0.82	0.0002275
NM_003665	Ficolin	0.52	0.0002861
NM_005514	MHC class IB	0.52	0.0005335
NM_033666	Integrin, beta 1 (fibronectin receptor, beta polypeptide)	0.40	0.0007798
NM_133503	Decorin	0.68	0.0011217
Signal transduction			
NM_004040	Ras homolog gene family, member B	0.25	<0.0000001
NM_003010	SAPK/Erk kinase 1	0.66	0.0000008
NM_000591	CD14 antigen	0.46	0.0000095
NM_004447	Epidermal growth factor receptor kinase substrate (Eps8)	0.64	0.0000166
NM_001175	Rho GDP dissociation inhibitor (GDI) beta	0.66	0.0000191
NM_001665	Ras homolog gene family, member G (rho G)	0.65	0.0000242
NM_002759	PKR	0.62	0.0000251
NM_080921	Protein tyrosine phosphatase, receptor type, c polypeptide	0.54	0.0001131
NM_000560	CD53 antigen	0.66	0.0001768
NM_033423	Granzyme H	0.77	0.0001909
NM_000064	Complement 3	0.52	0.0002377
NM_002576	p21-activated protein kinase (Pak1)	0.81	0.0004081
NM_000609	Intercrine-alpha (hIRH)	0.69	0.0004506
NM_006208	Phosphodiesterase I/nucleotide pyrophosphatase 1	0.70	0.0008048
NM_002659	Plasminogen	0.70	0.0035258
Metabolism			
NM_005891	Cytosolic acetoacetyl-coenzyme A thiolase	0.58	0.0000133
NM_000072	Fatty acid translocase (FAT/CD36)	0.69	0.0002073
NM_000175	Glucose phosphate isomerase	0.67	0.0004559
NM_000024	Adrenergic beta-2 receptor	0.63	0.0008699
NM_006430	Aspartylglucosaminidase	0.63	0.0015513
NM_013402	Fatty acid desaturase	0.60	0.0046714

Table 4. (continued)

GenBank Ref. Seq. ID	Gene	DM/ Non-DM	Parametric *p* value
Cytokine/growth factor-related			
NM_005228	Epidermal growth factor receptor (v-erb-b oncogene homolog)	0.64	0.0000001
NM_002087	Granulin	0.56	0.0000010
NM_000596	Insulin-like growth factor binding protein 1	0.16	0.0000013
NM_003242	Transforming growth factor, beta receptor IIB	0.50	0.0001222
NM_000416	Interferon gamma receptor 1	0.58	0.0001499
NM_000598	Insulin-like growth factor binding protein 3 precursor	0.58	0.0002442
NM_133484	TNF receptor-associated factor 2	0.65	0.0003767
Stress response			
NM_001461	Flavin-containing monooxygenase 5	0.41	0.0000081
NM_000940	Paraoxonase 3	0.65	0.0000222
NM_000636	Superoxide dismutase 2, mitochondrial	0.40	0.0001703
NM_001618	Poly(ADP-ribose) synthetase	0.75	0.0017561
Cell cycle/apoptosis/oncogenesis			
NM_006495	Ecotropic viral integration site 2B (EVI2B)	0.72	0.0000015
NM_001166	Baculoviral IAP repeat-containing protein 2	0.57	0.0000019
NM_003339	E2D2	0.66	0.0000081
NM_021960	Myeloid cell leukaemia sequence 1 (BCL2-related)	0.37	0.0000521
NM_002467	c-myc oncogene	0.61	0.0000620
NM_033355	FADD-homologous ICE/CED-3-like protease (FLICE)	0.69	0.0001103
NM_006826	14-3-3 protein TAU	0.65	0.0000472
NM_003932	Suppression of tumorigenicity 13 (colon carcinoma, Hsp70-interacting protein)	0.63	0.0003040

We identified 134 genes that were down-regulated in the livers of diabetic patients ($p<0.005$). Expressed sequence tags and genes with unknown function are not listed. DM, livers from Type 2 diabetic patients; Non-DM, livers from non-diabetic patients

like flavin containing monooxygenase (FMO) 5 and superoxide dismutase 2 (SOD2) (Table 4).

Real-time PCR analyses. Real-time PCR confirmed that expression of *BMP4* was significantly up-regulated in the livers of diabetic patients (Fig. 2a), with expression levels of *BMP4* as assessed by real-time PCR and cDNA microarray well correlated with each other ($r=0.58$, $p=0.0053$) (Fig. 2b). Real-time PCR also confirmed that the expression of endothelin and glutathione S-transferase T1 were up-regulated in the livers of diabetic patients (Fig. 2c, d). Because the microarray analysis was not sufficiently sensitive to detect *TGFB1* gene expression, we used real-time PCR to assay expression of this gene. As with other members of the TGF superfamily, expression of *TGFB1* message was up-regulated in the liver of diabetic patients, relative to that of non-diabetic patients (Fig. 2e).

Discussion

In assessing gene expression profiles in the livers of patients with and without Type 2 diabetes using cDNA microarray analyses and real-time quantitative PCR, we found that the twelve diabetic patients formed a separate cluster from the nine non-diabetic patients. This was especially evident in three subsets of differentially expressed genes encoding (i) transcription factors, (ii) cytokines and growth factors, and (iii) proteins associated with apoptosis. Diabetes is known to cause histological changes in the liver including NASH [13], and the difference in expression levels between diabetic and non-diabetic livers could therefore be related to these histological changes.

In the diabetes group, expression of 105 genes was significantly up-regulated, while expression of 134 genes was significantly down-regulated. Of those up-regulated, several belong to the TGF superfamily, including *BMP4*, *BMP7*, *TGFA* and *TGFB1*. Angiogenesis is an essential biological process, not only in embryogenesis but also in the progression of diabetic vascular complications. One member of the TGF superfamily, TGF-β, plays a critical role in angiogenesis [2], and also mediates expression of angiogenic factors such as *VEGF* [3], which we also found to be up-regulated in livers of diabetic patients. Another member, BMP-4, was recently found to stimulate VEGF synthesis [17, 18]. In development, VEGF acts upstream of the Notch pathway to determine arterial cell fate [19]. Notch signalling plays a critical role in vasculogenesis and angiogenesis [20]. In the absence of VEGF signalling, activation of the Notch pathway can rescue gene expression of arterial markers such as ephrin [20].

We also found that other cytokines involved in angiogenesis and the development of diabetic angi-

opathy, including endothelin [21] and *PDGF* [22], were up-regulated in diabetic livers. High concentrations of glucose enhance endothelin-1 expression, partly due to activation of protein kinase C, and may act to reduce retinal blood flow during the development of diabetic retinopathy [23]. In addition, receptors for PDGF and endothelin are up-regulated in the skeletal muscle of insulin-resistant Pima Indians [7]. Together, these alterations in gene expression in the diabetic liver could increase the risk for the systemic vascular complications associated with Type 2 diabetes, including diabetic retinopathy and ischaemic heart disease.

Plasmin is responsible for the proteolysis of extracellular matrix components, which prevent fibrosis and angiogenesis [24]. The down-regulation of plasminogen observed by us in the diabetic liver could thus result in reduced fibrinolysis, leading to thrombosis and atherosclerosis. Down-regulation of plasminogen has also been reported in the livers of ob/ob mice [11].

Recently, thrombospondin 2 gene polymorphism [25] and serum paraoxonase activity [26] were reported to predict coronary events. Mice deficient in thrombospondin 2 have a phenotype that could reduce the risk of myocardial infarction [27]. Thus the up-regulation of thrombospondin 2 and down-regulation of paraoxonase in the diabetic liver, as observed in this study, might be associated with increased risk of coronary artery disease.

Hyperglycaemia increases the production of reactive oxygen species, which may activate protein kinase C, induces advanced glycation end-product formation and activates the pleiotropic transcription factor, nuclear factor-kappa B [28]. Increases in reactive oxygen species are prevented by SOD2 [28]. Impaired expression of *SOD2* or other genes associated with a stress defence system, including *FMO5*, as observed here and in ob/ob mice [11], could increase oxidative stress in the diabetic state. Similar alterations in gene expression in blood vessels may increase the risk of atherosclerosis.

Several of the genes we found aberrantly expressed in livers of patients with Type 2 diabetes can also be altered in other organs of diabetic patients. For example, up-regulation of Rad (a Ras-oncogene associated with diabetes), heat shock 70kD protein, and receptors for PDGF and endothelin, and down-regulation of general transcription and translation factors, and of cadherin and *MHC* have been observed in the skeletal muscle of insulin-resistant Pima Indians [7] and in Type 2 diabetic patients [8]. In addition, up-regulation of epidermal growth factor receptor and down-regulation of fatty acid-associated enzymes, fibronectin, *VCAM1*, *MHC*, plasminogen, *SOD2*, *FMO5* and complement C3 have been observed in the liver of ob/ob mice [10, 11, 12].

We also observed, in the livers of Type 2 diabetic patients, reduced expression of the genes encoding some enzymes associated both with glucose metabolism (glucose phosphate isomerase, aspartylglucosaminidase and cytosolic acetoacetyl-coenzyme A thiolase) and with fatty acid metabolism (fatty acid desaturase and fatty acid translocase). Whilst this paper was being prepared, two other groups independently found a coordinated reduction of PGC1-responsive genes involved in oxidative metabolism in the skeletal muscle of Type 2 diabetic patients [29, 30]. A large-scale cDNA microarray containing comprehensive genes associated with metabolism could be used to find out whether these alterations also exist in the Type 2 diabetic liver.

In summary, the gene expression profile of Type 2 diabetic livers is different to that of the normal liver. Caution is necessary when generalising on the relevance of this observation for global cardiovascular complications. And while the direct contribution of these differential genes to systemic complications will, no doubt, be explained in the future, we suggest from our findings that clustering analyses and the identification of differentially expressed genes in the liver could be useful for clarifying the pathogenesis of Type 2 diabetes and its related complications.

Acknowledgements. We thank Dr Gen-ichi Nishimura and Professor Koichi Miwa from the Department of Surgery II, Kanazawa University for generously providing the liver tissue samples.

References

1. Expert committee on the diagnosis and classification of diabetes mellitus (2003) Report of the Expert Committee on the Diagnosis and Classification of Diabetes Mellitus. Diabetes Care 25:S5–S20
2. Larsson J, Goumans MJ, Sjostrand LJ et al. (2001) Abnormal angiogenesis but intact hematopoietic potential in TGF-beta type I receptor-deficient mice. Embo J 20:1663–1673
3. Pertovaara L, Kaipainen A, Mustonen T et al. (1994) Vascular endothelial growth factor is induced in response to transforming growth factor-beta in fibroblastic and epithelial cells. J Biol Chem 269:6271–6274
4. Schena M, Shalon D, Davis R, Brown P (1995) Quantitative monitoring of gene expression patterns with a complementary DNA microarray. Science 270:467–470
5. Honda M, Kaneko S, Kawai H, Shirota Y, Kobayashi K (2001) Differential gene expression between chronic hepatitis B and C hepatic lesion. Gastroenterology 120:955–966
6. Shirota Y, Kaneko S, Honda M, Kawai HF, Kobayashi K (2001) Identification of differentially expressed genes in hepatocellular carcinoma with cDNA microarrays. Hepatology 33:832–840
7. Yang X, Pratley RE, Tokraks S, Bogardus C, Permana PA (2002) Microarray profiling of skeletal muscle tissues from equally obese, non-diabetic insulin-sensitive and insulin-resistant Pima Indians. Diabetologia 45:1584–1593
8. Sreekumar R, Halvatsiotis P, Schimke JC, Nair KS (2002) Gene expression profile in skeletal muscle of type 2 diabetes and the effect of insulin treatment. Diabetes 51:1913–1920

9. Rome S, Clement K, Rabasa-Lhoret R et al. (2003) Microarray profiling of human skeletal muscle reveals that insulin regulates approximately 800 genes during a hyperinsulinemic clamp. J Biol Chem 278:18063–18068
10. Ferrante AW Jr, Thearle M, Liao T, Leibel RL (2001) Effects of leptin deficiency and short-term repletion on hepatic gene expression in genetically obese mice. Diabetes 50:2268–2278
11. Liang CP, Tall AR (2001) Transcriptional profiling reveals global defects in energy metabolism, lipoprotein, and bile acid synthesis and transport with reversal by leptin treatment in ob/ob mouse liver. J Biol Chem 276:49066–49076
12. Lan H, Rabaglia ME, Stoehr JP et al. (2003) Gene expression profiles of nondiabetic and diabetic obese mice suggest a role of hepatic lipogenic capacity in diabetes susceptibility. Diabetes 52:688–700
13. Reid AE (2001) Nonalcoholic steatohepatitis. Gastroenterology 121:710–723
14. Brunt EM, Janney CG, Di Bisceglie AM, Neuschwander-Tetri BA, Bacon BR (1999) Nonalcoholic steatohepatitis: a proposal for grading and staging the histological lesions. Am J Gastroenterol 94:2467–2474
15. Lee RG (1998) Alcoholic and nonalcoholic steatohepatitis pathology. In: Bloomer J, Goodman ZD, Ishak KG (eds) Clinical and pathological correlations in liver disease: approaching the next millennium. The Armed Forces Institute of Pathology, the American Registry of Pathology, the American Association for the Study of Liver Disease, Washington DC, pp 274–283
16. Ye QH, Qin LX, Forgues M et al. (2003) Predicting hepatitis B virus-positive metastatic hepatocellular carcinomas using gene expression profiling and supervised machine learning. Nat Med 9:416–423
17. Deckers MM, Bezooijen RL van, Horst G van der et al. (2002) Bone morphogenetic proteins stimulate angiogenesis through osteoblast-derived vascular endothelial growth factor A. Endocrinology 143:1545–1553
18. Tokuda H, Hatakeyama D, Shibata T, Akamatsu S, Oiso Y, Kozawa O (2003) p38 MAP kinase regulates BMP-4-stimulated VEGF synthesis via p70 S6 kinase in osteoblasts. Am J Physiol Endocrinol Metab 284:E1202–E1209
19. Lawson ND, Vogel AM, Weinstein BM (2002) Sonic hedgehog and vascular endothelial growth factor act upstream of the Notch pathway during arterial endothelial differentiation. Dev Cell 3:127–136
20. Liu ZJ, Shirakawa T, Li Y et al. (2003) Regulation of Notch1 and Dll4 by vascular endothelial growth factor in arterial endothelial cells: implications for modulating arteriogenesis and angiogenesis. Mol Cell Biol 23:14–25
21. Sarman B, Toth M, Somogyi A (1998) Role of endothelin-1 in diabetes mellitus. Diabetes Metab Rev 14:171–175
22. Inaba T, Ishibashi S, Gotoda T et al. (1996) Enhanced expression of platelet-derived growth factor-beta receptor by high glucose. Involvement of platelet-derived growth factor in diabetic angiopathy. Diabetes 45:507–512
23. Park JY, Takahara N, Gabriele A et al. (2000) Induction of endothelin-1 expression by glucose: an effect of protein kinase C activation. Diabetes 49:1239–1248
24. Blakesley VA (2000) The role of growth factors in the pathogenesis of diabetic microvascular complications. In: LeRoith D, Taylor SI, Olefsky JM (eds) Diabetes mellitus. A fundamental and clinical text. Lippincott Williams & Wilkins, Philadelphia, pp 1000–1008
25. Boekholdt SM, Trip MD, Peters RJ et al. (2002) Thrombospondin-2 polymorphism is associated with a reduced risk of premature myocardial infarction. Arterioscler Thromb Vasc Biol 22:e24–e27
26. Mackness B, Durrington P, McElduff P et al. (2003) Low paraoxonase activity predicts coronary events in the Caerphilly Prospective Study. Circulation 107:2775–2779
27. Kyriakides TR, Zhu YH, Smith LT et al. (1998) Mice that lack thrombospondin 2 display connective tissue abnormalities that are associated with disordered collagen fibrillogenesis, an increased vascular density, and a bleeding diathesis. J Cell Biol 140:419–430
28. Nishikawa T, Edelstein D, Du XL et al. (2000) Normalizing mitochondrial superoxide production blocks three pathways of hyperglycaemic damage. Nature 404:787–790
29. Patti ME, Butte AJ, Crunkhorn S et al. (2003) Coordinated reduction of genes of oxidative metabolism in humans with insulin resistance and diabetes: Potential role of PGC1 and NRF1. Proc Natl Acad Sci USA 100:8466–8471
30. Mootha VK, Lindgren CM, Eriksson KF et al. (2003) PGC-1alpha-responsive genes involved in oxidative phosphorylation are coordinately downregulated in human diabetes. Nat Genet 34:267–273

[CANCER RESEARCH 64, 3326–3333, May 1, 2004]

Different Procarcinogenic Potentials of Lymphocyte Subsets in a Transgenic Mouse Model of Chronic Hepatitis B

Yasunari Nakamoto,[1] Takashi Suda,[2] Takashi Momoi,[3] and Shuichi Kaneko[1]

[1]Department of Gastroenterology, Graduate School of Medicine, [2]Center for the Development of Molecular Target Drugs, Cancer Research Institute, Kanazawa University, Kanazawa, and [3]Division of Development and Differentiation, National Institute of Neuroscience, NCNP, Kodaira, Tokyo, Japan

ABSTRACT

The immune response to hepatitis viruses is believed to be involved in the development of chronic hepatitis; however, its pathogenetic potential has not been clearly defined. The current study, using a transgenic mouse model of chronic hepatitis B, was designed to determine the relative contributions of the immune cell subsets to the progression of liver disease that induces hepatocellular carcinogenesis. Hepatitis B virus transgenic mice were adoptively transferred with $CD4^+$ and $CD8^+$ T cell-enriched or -depleted and B cell-depleted splenocytes obtained from hepatitis B surface antigen-primed, syngeneic nontransgenic donors. The resultant liver disease, hepatocyte apoptosis, regeneration, and tumor development were assessed and compared with the manifestations in mice that had received unfractionated spleen cells. Transfer of $CD8^+$-enriched splenocytes caused prolonged disease kinetics, and a marked increase in the extent of hepatocyte apoptosis and regeneration. In 12 of 14 mice the transfer resulted in multiple hepatocellular carcinomas (HCCs) comparable with the manifestations seen in the mice transferred with total splenocytes. In contrast, mice that had received $CD4^+$-enriched cells demonstrated lower levels of liver disease and developed fewer incidences of HCC (4 of 17). The experiment also revealed that all of the groups of mice complicated with HCC developed comparable mean numbers and sizes of tumors. B-cell depletion had no effect on disease kinetics in this model. Taken together, these results demonstrate that the pathogenetic events induced by $CD8^+$ T-cell subset are primarily responsible for the induction of chronic liver disease that increases tumor incidence, suggesting their potential in triggering the process of hepatocarcinogenesis.

INTRODUCTION

Hepatocellular carcinoma (HCC) occurs after many years of chronic hepatitis (1, 2). During the process, both viral and host factors have been implicated in liver cell transformation and carcinogenesis. On the one hand, some viral proteins, *i.e.*, hepatitis B virus (HBV) X protein (3, 4) and hepatitis C virus core protein (5, 6), are considered to contribute to tumor development in the liver, because high-level expression of the proteins increases the incidence of HCC in transgenic mice. Furthermore, most tumors contain clonally integrated HBV DNA and microdeletions in the flanking cellular DNA, which could theoretically deregulate cellular growth control mechanisms (7). And COOH-terminally truncated viral envelop proteins expressed from integrated subviral DNA may have transactivating activity (8, 9) and could potentially contribute to carcinogenesis in chronic HBV infection.

On the other hand, prolonged inflammation is thought to set up a cycle of liver cell destruction and regeneration, resulting in a mitogenic and mutagenic environment that can precipitate random genetic and chromosomal damage, and lead to the development of HCC (10–12). In patients with chronic hepatitis B and C, $CD4^+$ and $CD8^+$ T lymphocytes specific for the viruses are detectable in the peripheral blood and in intrahepatic infiltrates, and are suggested to play a role in the immune pathogenesis of liver disease (13–16). Furthermore, transfer of the virus-specific $CD4^+$ and $CD8^+$ T-cell clones was observed to induce acute necroinflammatory liver disease in the models of HBV transgenic mice (17–20). However, the relative contribution of $CD4^+$ and $CD8^+$ T lymphocytes to the induction of chronic liver cell injury was not determined, because the T-cell clones induced neither prolonged liver diseases nor HCC in the models of acute hepatocellular injury, and because the animal model that pathophysiologically reproduces human chronic viral hepatitis was not available. In an effort to clarify the carcinogenic potential of chronic inflammation, we have developed a model of chronic immune-mediated liver disease using HBV transgenic mice that express the envelop proteins in the hepatocytes (21). The results demonstrate that continuous intrahepatic inflammation is sufficient to cause liver cancer in the absence of pre-existing viral transactivation, insertional mutagenesis, or genotoxic chemicals during chronic HBV infection.

We have shown recently that the administration of anti-Fas ligand (FasL) neutralizing antibody reduces hepatocyte apoptosis, proliferation, and liver inflammation, and eventually diminishes the development of HCC. This observation suggests a critical involvement of FasL-induced pathogenetic events in the process of hepatocarcinogenesis (22). We have also reported evidence that the FasL-dependent pathway is critically involved in the development of acute liver cell injury induced by $CD8^+$ cytotoxic T-lymphocyte (CTL) clones (23, 24). Because FasL is known to be expressed on activated T lymphocytes (25–29), we speculated that the $CD8^+$ T-cell subset was implicated as a causative factor responsible for the chronic liver cell injury that promotes hepatocarcinogenesis.

To determine the involvement of immune cell subsets in the progression of chronic liver disease, the current experiment was performed in the model of chronic immune-mediated hepatitis in which T- and B-cell subset-depleted or -enriched splenocytes obtained from HBV-primed, nontransgenic mice were transferred into the transgenic recipients, and liver disease and tumor development were monitored. The results demonstrate that each cell subset causes unique kinetics of liver disease and different incidence of liver cancer.

MATERIALS AND METHODS

HBV Transgenic Mice. Hepatitis B surface antigen (HBsAg) transgenic mouse lineage 107–5D [official designation Tg(Alb-1, HBV)Bri66; inbred B10D2, $H\text{-}2^d$] was kindly provided by Dr. Francis V. Chisari (The Scripps Research Institute, La Jolla, CA; Ref. 30). Lineage 107–5D contains the entire HBV envelope coding region (subtype ayw) under the constitutive transcriptional control of the mouse albumin promoter (30). These mice express the HBV small, middle, and large envelope proteins in their hepatocytes (30, 31), they are immunologically tolerant to HBsAg at the T-cell level (32), and they display no evidence of liver disease during their lifetime although they do develop "ground glass" hepatocytes due to overexpression of the large envelope protein (30). There is no X-RNA or X-protein expression detectable in the livers of these animals.[4] Importantly, the mice develop a severe MHC class I-restricted necroinflammatory liver disease after the adoptive transfer of HBsAg-specific CTLs (17, 18, 30).

Received 12/6/03; revised 2/5/04; accepted 2/25/04.

The costs of publication of this article were defrayed in part by the payment of page charges. This article must therefore be hereby marked *advertisement* in accordance with 18 U.S.C. Section 1734 solely to indicate this fact.

Requests for reprints: Shuichi Kaneko, Department of Gastroenterology; Graduate School of Medicine, Kanazawa University; 13-1 Takara-machi, Kanazawa 920-8641, Japan. Phone: 81-76-265-2231; Fax: 81-76-234-4250; E-mail: skaneko@medf.m.kanazawa-u.ac.jp.

[4] Unpublished observations.

Disease Model. To break tolerance at the B- and T-cell levels, HBV transgenic mice were thymectomized, bone marrow-reconstituted, and adoptively transferred with nontransgenic immune systems according to the procedures described previously (21, 33). Briefly, 8–10-week-old male transgenic mice were thymectomized. Seven days later the mice were irradiated (900 cGy) and then reconstituted by the i.v. injection of 10^7 bone marrow cells collected from the femurs and tibias of syngeneic nontransgenic B10D2 (H-2^d) mice. One week after the bone marrow transfer, the animals were injected i.v. with the indicated numbers of splenocyte subsets from nontransgenic B10D2 (H-2^d) mice that were infected i.p. with a recombinant vaccinia virus expressing HBsAg (HBs-vac) 3 weeks before the splenocyte transfer (17). At the same time, transfer of total splenocytes from the primed nontransgenic mice and the unprimed transgenic littermates were performed for control purposes. The resultant hepatocellular injury was monitored biochemically as serum alanine aminotransferase (ALT) activity (10). Results were expressed as mean units per liter ± SE of serum ALT activity, and differences between groups were assessed for statistical significance by Student's *t* test. Tumor development was assessed by abdominal palpation and confirmed by autopsy at which time the number of tumors visible at the surface of each liver was counted, and the diameter of each tumor was measured with a millimeter rule. All of the experiments satisfied the Guidelines for the Care and Use of Laboratory Animals in Takara-machi Campus of Kanazawa University.

Depletion and Enrichment of T- and B-Cell Subsets. To deplete $CD4^+$ or $CD8^+$ T cells, splenocytes were treated with monoclonal antibodies (mAbs) specific for CD4 (GK1.5) or CD8 (2.43; American Type Culture Collection, Manassas, VA), respectively, and then with rabbit complement (Cedarlane, Hornby, Ontario, Canada). B cells of splenocytes were depleted on the Mouse T Cell immunocolumn (Cytovax, Edmonton, Alberta, Canada), by treatment with mAb specific for MHC class II I-A^d (MK-D6; American Type Culture Collection), and with rabbit complement. To enrich $CD4^+$ or $CD8^+$ T cells, splenocytes were passed over the Mouse T Cell immunocolumn and treated with a combination of anti-CD8 and anti-I-A^d mAbs, or anti-CD4 and anti-I-A^d mAbs, respectively, and then with rabbit complement. The purity of the T- and B-cell populations was monitored by immunolabeling with FITC-conjugated rat mAb specific for mouse CD4 (RM4–5; BD PharMingen, San Diego, CA), and phycoerythrin-conjugated rat mAb specific for mouse CD8 (53–6.7), or CD19, which is a B cell-specific transmembrane protein (1D3; BD PharMingen), followed by fluorescence-activated cell sorter analysis.

Immunohistochemical Analysis. Tissue samples were fixed in buffered zinc formalin (Anatech Ltd., Battle Creek, MI), embedded in paraffin, sectioned (at 3 μ m), and stained with H&E as described previously (21). Some of the paraffin sections were treated with anti-proliferating cell nuclear antigen (PCNA) and anti-HBsAg primary solutions (Dako, Carpinteria, CA) at 1:10 and 1:1000 dilutions, respectively, followed by biotin-conjugated secondary antibody (Vector Laboratories, Inc., Burlingame, CA; Ref. 34). $PCNA^+$ and $HBsAg^+$ cells were then visualized using a VECTASTAIN ABC Standard kit (Vector Laboratories), and the tissue sections were counterstained with hematoxylin before mounting. Liver tissue samples were also embedded in OCT compound (Sakura Finetek, Torrance, CA) and snap-frozen in liquid nitrogen. Cryostat sections of frozen tissues were fixed in 4% paraformaldehyde overnight at 4°C. After blocking biotin, the tissue sections were incubated with rabbit antimouse active caspase-3 antibodies (35) at a 1:400 dilution for 30 min at room temperature, followed by biotin-conjugated goat antirabbit IgG secondary antibodies (Vector Laboratories). The reaction was visualized in the same way as the PCNA staining described above. Terminal deoxynucleotidyl transferase-mediated nick end labeling (TUNEL) analysis was performed on serial liver sections according to the manufacturer's instructions (Roche, Indianapolis, IN).

RESULTS

Cellular Basis for Prolonged Chronic Immune-Mediated Hepatitis in HBV Transgenic Mice. To determine the relative contribution of immune cell subsets to prolonged chronic immune-mediated hepatitis in HBV transgenic mice, the splenocytes isolated from HBsAg-primed nontransgenic mice were depleted (Fig. 1) or enriched (Fig. 2) of $CD4^+$ and $CD8^+$ T cells and $CD19^+$ B cells, and they were then adoptively transferred into thymectomized, bone marrow-reconstituted HBV transgenic recipients. The kinetics of all of the disease manifestations was compared with that caused by total splenocyte transfer. As observed previously (21), total cell transfer caused prolonged chronic hepatitis (Fig. 1). Briefly, serum ALT activity increased from preinjection levels of 20–40 units/liter to approximately 2000–4000 units/liter within 7 days after adoptive transfer and fell progressively thereafter. Importantly, the ALT activity never returned to baseline in these animals, remaining at least two to three times above normal throughout the experiment. B cell-depleted splenocytes demonstrated disease kinetics comparable with that seen after total cell transfer. Similarly, $CD4^+$ subset-depleted splenocytes caused acute elevation of serum ALT activity within 7 days after the transfer, and the animals developed persistent liver disease, although the peak of disease activity was lower than that seen after total cell transfer. In contrast, $CD8^+$ subset depletion markedly reduced the peak and diminished the disease activity in the chronic phase later than 7 days. In addition, we assume that a contaminating 1.4% (1.3×10^6) of $CD8^+$ T cells in this $CD8^+$ subset-depleted population may not influence the kinetics of liver disease, because we observed that transfer of 1×10^7 total splenocytes, which contained ~20% (2×10^6) $CD8^+$ T cells, did not cause elevation of ALT in this model.[4]

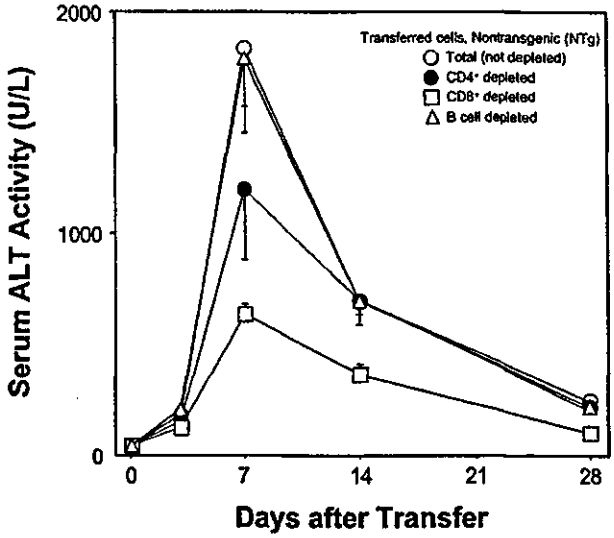

Fig. 1. Kinetics of serum alanine aminotransferase (*ALT*) after transfer of $CD4^+$ T cell-depleted, $CD8^+$ T cell-depleted, or B cell-depleted splenocytes in a transgenic mouse model of chronic hepatitis B. The splenocytes were obtained from hepatitis B surface antigen-primed, syngeneic nontransgenic mice. Nine $\times$ 10^7 cells of the splenocytes depleted of $CD4^+$ [$CD4^+$, 1.4%; $CD8^+$, 20.8%; B ($CD19^+$), 32.4%], $CD8^+$ ($CD4^+$, 15.0%; $CD8^+$, 1.4%; B, 28.5%), or B cells ($CD4^+$, 17.5%; $CD8^+$, 38.5%; B, 0.1%) were transferred into hepatitis B virus transgenic mice. At the same time, transfer of the total splenocytes (1×10^8 cells; $CD4^+$, 12.7%; $CD8^+$, 16.7%; B, 26.8%) was performed for control purposes. The serum ALT activity (mean units/liter) was monitored to evaluate liver injury; *bars*, ±SE. Each group represents 5 animals.

Consistent with the differences in the kinetics of liver disease induced by the subset-depleted cells, transfer of $CD8^+$ subset-enriched splenocytes displayed the prolonged kinetics comparable with total cell transfer except for the lower peak of ALT (Fig. 2). In contrast, $CD4^+$ subset-enriched cells caused a transient elevation of ALT 7 days after adoptive transfer that seemed to improve 14 days after the transfer. In addition, we confirmed that transgenic splenocytes induce no disease in the recipient mice, indicating that all subsets of transgenic splenocytes are perfectly immunologically tolerant to the viral antigens as observed previously (21). Whereas these subset-enriched splenocytes included unidentified non-T and non-B cells that might influence the kinetics of liver disease, the data collectively demonstrate that $CD8^+$ T lymphocytes contributed not

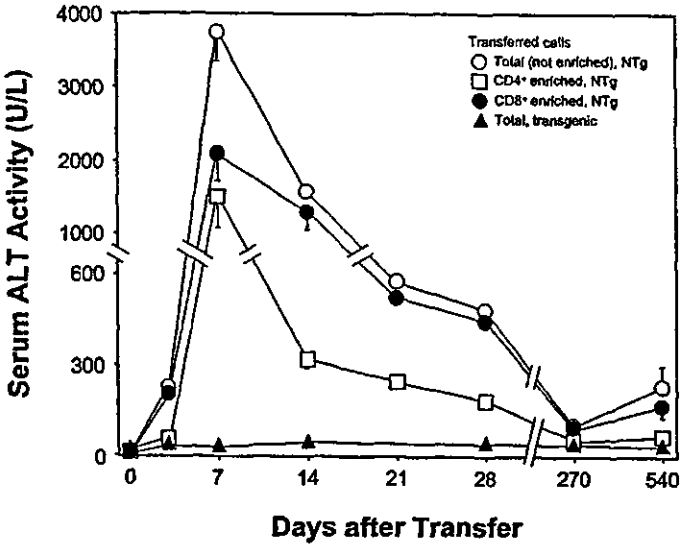

Fig. 2. Kinetics of serum alanine aminotransferase (*ALT*) after transfer of $CD4^+$ or $CD8^+$ T cell-enriched splenocytes in a transgenic mouse model of chronic hepatitis B. The splenocytes were obtained from hepatitis B surface antigen-primed, syngeneic nontransgenic mice. Five $\times 10^7$ cells of the splenocytes enriched for $CD4^+$ ($CD4^+$, 78.7%; $CD8^+$, 1.8%; B, 0.9%) or $CD8^+$ ($CD4^+$, 2.0%; $CD8^+$, 84.2%; B, 0.7%) were transfused into hepatitis B virus transgenic mice. At the same time, transfer of total splenocytes from the primed nontransgenic mice (1×10^8 cells; $CD4^+$, 10.4%; $CD8^+$, 21.3%; B, 23.0%) and the unprimed transgenic littermates (1×10^8 cells) were performed for control purposes. The serum ALT activity (*mean units/liter*) was monitored to evaluate liver injury; *bars*, ±SE. Each group represents 5 animals. Similar experiments were performed three times and representative data are shown.

only to the induction of hepatocellular injury but also to the maintenance of disease activity in the HBV transgenic mouse model.

In the analysis of liver histology (Fig. 3, *A* and *B*) the mice transferred with total splenocytes and with $CD8^+$ subset-enriched cells demonstrated severe infiltration of inflammatory cells, apoptotic and necrotic hepatocytes, many necroinflammatory foci, and mitotic figures. In contrast, the liver samples of mice transferred with the $CD4^+$ subset-enriched cells showed reduced infiltration of inflammatory cells, and minimal induction of apoptosis and liver cell injury. Consistent with the differences in disease activity revealed by the change in the serum ALT level, the results indicate that the $CD8^+$ subset was critically involved in the histological changes of pathological features associated with the establishment of prolonged chronic hepatitis seen in this model.

Apoptosis and Regeneration of Hepatocytes Induced by Differential Immune Cell Subsets in Prolonged Chronic Liver Disease. To monitor the hepatocyte destruction and regeneration caused by inflammation with immune cell subsets, the activation of the caspase cascade was determined immunohistochemically using mAb specific for the activated form of caspase-3. Degradation of DNA from apoptotic hepatocytes was measured by nuclear staining using the TUNEL method, and hepatocyte proliferation was assessed with mAb specific for PCNA (Fig. 4, *A* and *B*). Consistent with the differences in the serum levels of ALT activity, $CD8^+$ subset-enriched splenocytes induced marked caspase-3 activation and DNA degradation, comparable with the effects seen with total splenocytes, whereas CD4 enrichment diminished the number of active caspase-3^+ and $TUNEL^+$ hepatocytes. A pair of serial sections in mirror-image orientation stained with antiactive caspase-3 antibodies and the TUNEL method revealed that strong caspase-3 activation and DNA degradation were occurring in hepatocytes along the edge of the area where massive infiltrating cells were found. These data suggest that massive hepatocyte apoptosis may be caused by extensive infiltration of the transferred $CD8^+$ splenocyte subset into the liver tissues. In addition, the observation at the single cell level indicated that the hepatocytes stained by the antiactive caspase-3 and by the TUNEL method did not seem to perfectly coincide. We speculate that this could be due to the difference in the phase of apoptotic process, because caspase activation and DNA degradation may be detected in the earlier and the later phases by the two independent methods, respectively.

We also observed many $PCNA^+$ hepatocytes when total and $CD8^+$ subset-enriched splenocytes were transferred. In contrast, we found only a few $PCNA^+$ hepatocytes in mice transfused with $CD4^+$ cells, where most of the $PCNA^+$ cells were infiltrating inflammatory cells. Taken together, these results indicate that $CD8^+$ T cells played a major role in induction of hepatocyte apoptosis and regenerative hepatocyte proliferation in this hepatitis model; $CD4^+$ T cells did, however, play a minor role, especially in an early period of the acute phase.

Hepatocarcinogenesis Associated with Prolonged Chronic Liver Disease Induced by Differential Immune Cell Subsets. We have reported that HCC development was primarily dependent on prolonged chronic inflammation in the liver after transfer of HBsAg-primed, total splenocytes (21). To evaluate the relative procarcinogenic potential of liver disease induced by differential immune cell subsets, tumor development was monitored for 11–22 months in the mice transferred with the primed splenocyte subsets (Table 1). Twelve of the 14 animals transferred with $CD8^+$ subset-enriched splenocytes developed HCC, the incidence of which was comparable with that seen after total cell transfer (11 of 12; Refs. 21, 22). Most of them displayed multiple tumors, the size of the largest tumor was ranging up to 20 mm in diameter, and they illustrated the classical histological features of well-differentiated HCC including clear cells (Fig. 5, *A* and *F*). The surrounding hepatic parenchyma displayed focal lobular inflammatory infiltrates associated with degenerating hepatocytes, marked lobular disarray, fatty deposits, and clear tumor cell nests. The expression of HBsAg was abolished or decreased to a great extent in the tumor cells probably due to the altered transcription state (10, 11), whereas it was detectable in the surrounding parenchyma (Fig. 5, *B* and *G*). Even in the surrounding tissue the levels of expression were diminished, which was presumably due to long-term persistent inflammatory stimulation via noncytolytic cytokine-dependent mechanisms (36, 37). In addition, well-differentiated HCC consisting of tumor cells with large amounts of fatty deposits (Fig. 5*C*) were seen in the same liver tissue of the mouse indicated in Fig. 5*A*, suggesting a high potential for tumorigenesis induced by chronic immune-mediated liver disease. In tumor tissues of the mice transferred with $CD8^+$ subset-enriched cells, we observed both highly differentiated, fat deposited neoplastic hepatocytes (Fig. 5*H, right area*) and poorly differentiated, sarcomatous components (Fig. 5*H, left area*). Furthermore, 2 of the mice were complicated with the rupture of HCC and bloody ascites (Fig. 5, *I* and *J*). All of the data indicate that prolonged chronic inflammation caused by the $CD8^+$ subset displayed virtually the same effects as that by total splenocytes on the induction of hepatocarcinogenesis.

In contrast, the animals transferred with $CD4^+$ subset-enriched splenocytes displayed a lower potential for hepatocarcinogenesis, in which 4 of the 17 mice developed HCC (Table 1). However, the tumors were histologically identical to those in the animals transferred with total splenocytes (Fig. 5, *D* and *E*). Interestingly, the numbers and sizes of tumors were comparable among the mice complicated with HCC after the transfer with total, $CD4^+$, or $CD8^+$ subset-enriched splenocytes [numbers of liver tumors/sizes (*mm*) in diameter of largest tumors (means ± SE); 4.2 ± 2.1/8.9 ± 1.7, 3.3 ± 1.3/7.8 ± 2.4, and 3.0 ± 0.7/10.2 ± 1.0, respectively; $P > 0.5$] (Table 1). The data indicate that the pathogenetic events induced by individual

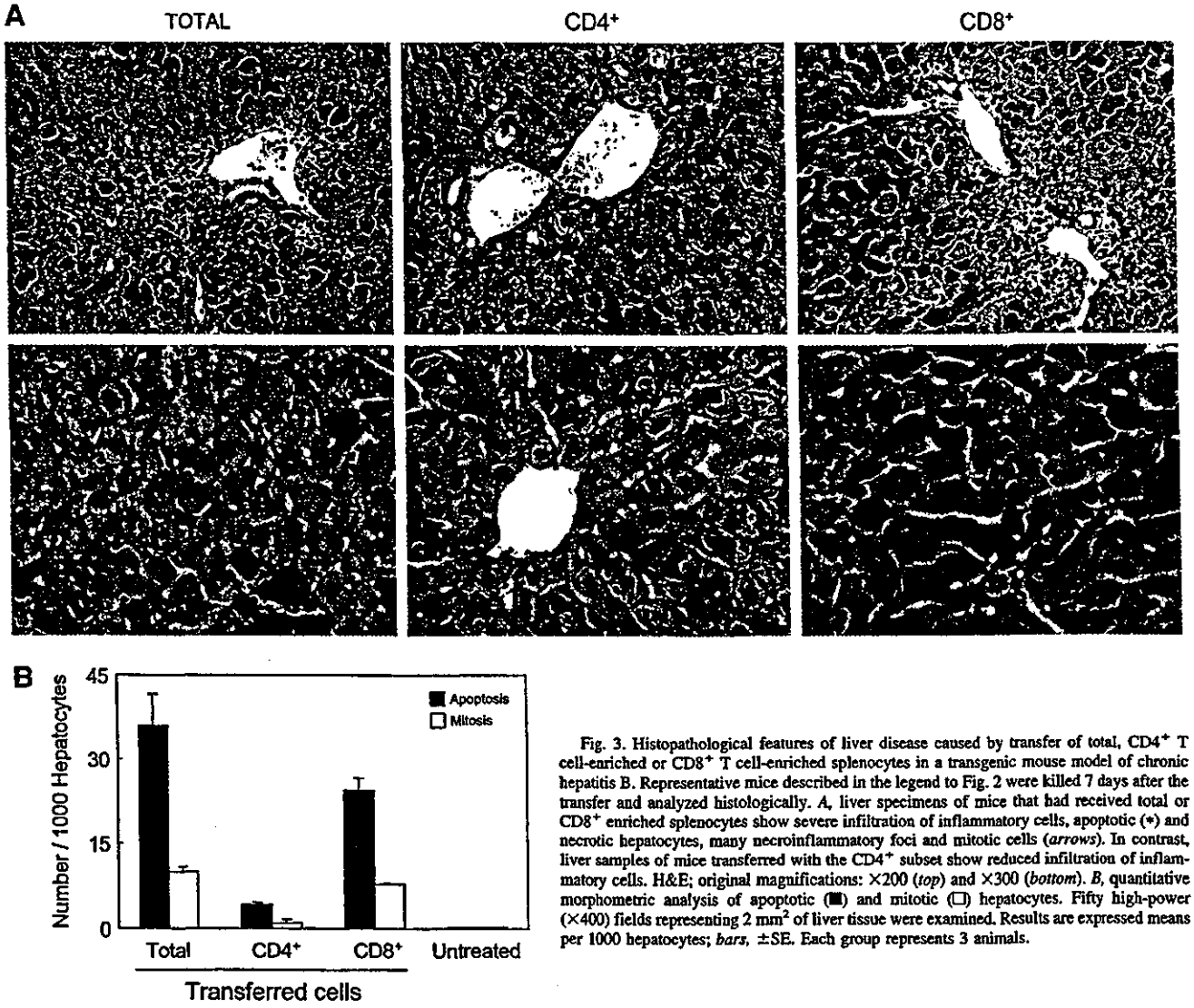

Fig. 3. Histopathological features of liver disease caused by transfer of total, $CD4^+$ T cell-enriched or $CD8^+$ T cell-enriched splenocytes in a transgenic mouse model of chronic hepatitis B. Representative mice described in the legend to Fig. 2 were killed 7 days after the transfer and analyzed histologically. *A*, liver specimens of mice that had received total or $CD8^+$ enriched splenocytes show severe infiltration of inflammatory cells, apoptotic (•) and necrotic hepatocytes, many necroinflammatory foci and mitotic cells (*arrows*). In contrast, liver samples of mice transferred with the $CD4^+$ subset show reduced infiltration of inflammatory cells. H&E; original magnifications: ×200 (*top*) and ×300 (*bottom*). *B*, quantitative morphometric analysis of apoptotic (■) and mitotic (□) hepatocytes. Fifty high-power (×400) fields representing 2 mm^2 of liver tissue were examined. Results are expressed means per 1000 hepatocytes; *bars*, ±SE. Each group represents 3 animals.

T-cell subsets influenced the potential in triggering the process of hepatocarcinogenesis rather than promoting tumor growth thereafter, resulting in different incidence of liver tumor. In addition, the mice thymectomized, irradiated, and transferred with splenocytes from the syngeneic transgenic animals or the unmanipulated controls developed no liver tumors. Collectively, the results demonstrate that each subset of the immune cells may individually contribute to the HCC development in this model. The $CD8^+$ subset plays a primary role in the maintenance of chronic liver disease and induction of liver tumors, whereas the $CD4^+$ subset displays a minimal potential for tumorigenesis during the process of prolonged chronic inflammation in the liver.

DISCUSSION

The current study indicates that T cells, especially the $CD8^+$ subset, rather than B cells are primarily responsible for the induction of prolonged liver injury in a mouse model of viral hepatitis. In contrast to the $CD8^+$ T-cell subset, $CD4^+$ T cells caused milder hepatic injury that seemed to improve shortly after the transfer as seen at the transaminase level. Consistent with the severity and duration of persistent liver disease, $CD8^+$ T cells displayed strong induction of hepatocellular apoptosis, inflammation, and regenerative proliferation that sets up a cycle of liver cell destruction and regeneration. Furthermore, the pathogenetic events induced by individual T-cell subsets exerted their different potential in triggering the oncogenic process of hepatocarcinogenesis. On the basis of these results, we suggest that $CD8^+$ T lymphocytes can principally contribute to the progression of chronic liver disease and the initiation of a complex sequence of events that leads to the development of HCC.

In the previous study, we observed that $CD8^+$ CTL clones caused liver cell apoptosis by activating the FasL/Fas-, perforin/granzyme-, and cytokine-dependent death pathways in the model of acute hepatocellular injury (24). Additionally, the liver cell injury was amplified by inflammation that may be exaggerated by FasL expressed on $CD8^+$ CTL clones (18, 19). Similarly, the histological findings in the current study indicated that an intracellular caspase cascade, which is a death pathway of hepatocytes, was strongly activated after $CD8^+$ T-cell transfer, and hepatocyte apoptosis was detectable along the area with inflammatory infiltrates. The massive cell loss through inflammation was thought to stimulate the regenerative proliferation of hepatocytes. These data suggest that the effector mechanism for chronic liver disease induced by $CD8^+$ T cells may be similar to acute liver cell injury induced by the CTL clones.

In other mouse models, liver cell injury was induced by transfer of $CD8^+$ CTL clones or hepatotoxic agents, and demonstrated

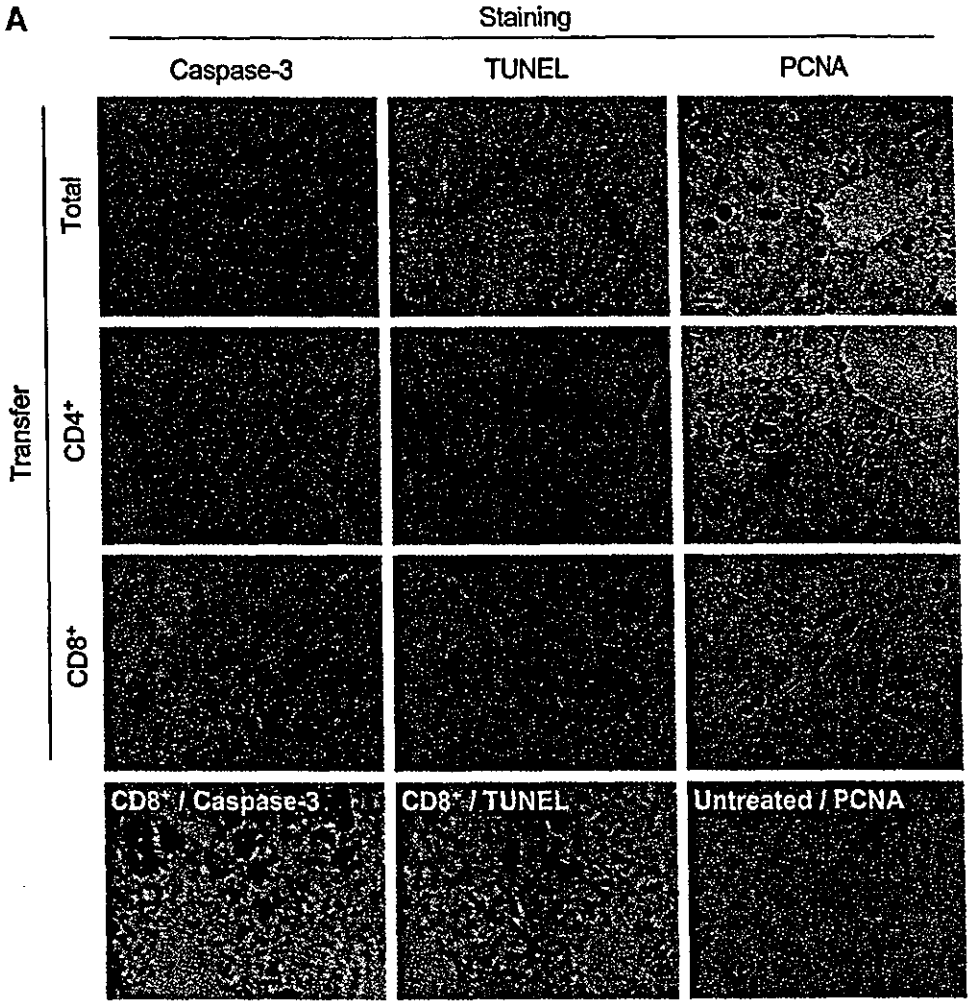

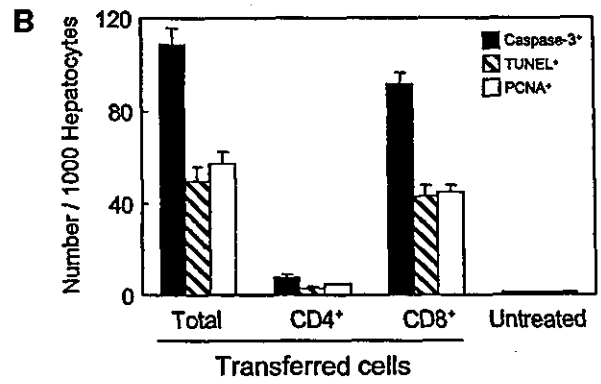

Fig. 4. Immunohistochemical analysis of hepatocellular apoptosis and regeneration induced by transfer of total, $CD4^+$ T cell-enriched or $CD8^+$ T cell-enriched, splenocytes in a transgenic mouse model of chronic hepatitis B. Representative mice described in the legend to Fig. 2 were killed 7 days after the transfer. *A*, immunohistochemical analysis of active caspase-3 and terminal deoxynucleotidyl transferase-mediated nick end labeling (TUNEL) analysis were performed in mirror-image serial sections of the liver tissues. $TUNEL^+$ hepatocyte nuclei are indicated with *arrows*. Proliferating cell nuclear antigen (PCNA) expression was analyzed in the same tissues. Age-matched, untreated hepatitis B virus transgenic mouse liver was stained for PCNA as a control. Original magnifications, ×40 (*top three panels* of caspase-3 and TUNEL staining; *bar* represents 200 μ m), and ×400 (the *other panels*: *bar* represents 20 μm). *B*, quantitative morphometric analysis of caspase-3^+ (■), $TUNEL^+$ (▨) and $PCNA^+$ (□) hepatocytes. Fifty high-power (×400) fields representing 2 mm^2 of liver tissue were examined. Results are expressed means per 1000 hepatocytes; *bars*, ±SE. Each group represents 3 animals.

acute, self-limited kinetics (17, 18, 30, 38). In the current experiment, prolonged immune-mediated hepatitis was established after transfer of $CD8^+$ T cells obtained from HBsAg-primed, nontransgenic mice to the transgenic recipients. We speculated that the transferred, $CD8^+$ T cells primarily contributed to the unique kinetics of liver disease because the $CD8^+$ subset of splenocytes were prepared without an *in vitro* stimulation, indicating that not only effector but also memory T cells were included in the transplanted cells. $CD8^+$ memory T cells were reported recently to have a longer life span than $CD4^+$ memory T cells (39). Thus, the lymphocytic choriomeningitis virus-specific $CD8^+$ T cells appeared to survive in secondary lymphoid organs (periphery) and display their antiviral effects for >2 years (40–42). Consistent with this finding, we observed previously that the HBsAg-specific, $CD8^+$ CTL response was detected in the splenocytes 17 months after adoptive transfer in this chronic disease model (21). Collectively, the transferred, memory $CD8^+$ T cells are estimated to home to and survive in secondary lymphoid organs for >1 and 1.5 years, and suggested to continuously supply effector T cells into liver tissue through blood flow, which can recognize HBsAg expressed on the hepatocytes and maintain hepatocellular injury.

During the carcinogenetic process, it has been suggested that latent genetic mutations in the cells can be induced to undergo clonal selection in the initiation stage, and that the growth of the initiated cells that carry the first mutation can be stimulated in the promotion stage (43). Accordingly, the oncogenic potential in the initiation and

Table 1 *Hepatocarcinogenesis after transfer of differential immune cell subsets*

Mouse ID	Months after spl.[a] transfer	Age (mo.) at killing	No. of tumors	Largest tumor (mm)[b]	Tumor histology
Transferred with total, HBsAg-primed nontransgenic splenocytes (1×10^8 cells; $CD4^+$, 10.4%; $CD8^+$, 21.3%; B, 23.0%)					
46	22	24	1	10	HCC
56	16	19	3	10	HCC
60	18	21	2	20	HCC
85	18	21	3	3	HCC
88	17	20	1	4	HCC
131	17	19	2	8	HCC
185	11	14	3	3	HCC
198	15	18	1	3	Adenoma
227	13	16	1	5	HCC
269	15	18	>25[c]	15	HCC
265	15	18	4	5	HCC
280	21	23	1	15	HCC
Mean (range)	16.5 (11–22)	19.3 (14–24)	3.9 (1–25<)	8.4 (3–20)	
Transferred with $CD4^+$ T cell-enriched, HBsAg-primed nontransgenic splenocytes (5×10^7 cells; $CD4^+$, 78.7%; $CD8^+$, 1.8%; B, 0.9%)					
98	16	19	0	0	
99	17	20	2	6	HCC
137	15	17	0	0	
172	19	22	0	0	
201	15	18	0	0	
202	12	15	0	0	
211	17	19	2	2	Adenoma
248	14	17	0	0	
275	22	25	3	15	HCC
276	15	18	0	0	
304	18	21	1	5	HCC
305	18	21	7	5	HCC
307	18	21	0	0	
308	18	21	0	0	
322	18	20	0	0	
323	18	20	0	0	
327	18	20	1	3	Adenoma
Mean (range)	16.9 (12–22)	19.6 (15–25)	0.9 (0–7)	2.1 (0–15)	
Transferred with $CD8^+$ T cell-enriched, HBsAg-primed nontransgenic splenocytes (5×10^7 cells; $CD4^+$, 2.0%; $CD8^+$, 84.2%; B, 0.7%)					
91	17	20	1	10	HCC
132	18	20	8	15	HCC
209	18	21	3	8	HCC
224	12	15	3	5	HCC
225	16	19	1	7	HCC
283	14	16	1	17	HCC
313	18	21	2	10	HCC
314	16	19	5	10	HCC
316	18	21	6	7	HCC
296	16	19	1	9	HCC
334	18	20	0	0	
335	18	20	1	14	HCC
338	18	20	4	10	HCC
298	18	21	1	3	Adenoma
Mean (range)	16.8 (12–18)	19.4 (15–21)	2.6 (0–8)	8.9 (0–17)	
Transferred with total (1×10^8 cells; $CD4^+$, 17.5%; $CD8^+$, 11.7%; B, 25.8%)					
142[d]	19	22	0	0	
147[d]	19	22	0	0	
152[d]	15	18	0	0	
161[d]	12	15	0	0	
9[e]	0	17	0	0	
220[e]	0	17	0	0	
221[e]	0	18	0	0	
233[e]	0	19	0	0	
254[e]	0	20	0	0	
368[e]	0	20	0	0	
369[e]	0	21	0	0	
235[e]	0	22	0	0	
236[e]	0	22	0	0	
238[e]	0	23	0	0	
288[e]	0	24	0	0	
Mean (range)	ND	20.0 (15–24)	0	0	

[a] spl., splenocyte; HBsAg, hepatitis B surface antigen; ND, not determined; HCC, hepatocellular carcinoma.
[b] Diameter in the major axis.
[c] Attributed to 25 for statistical analysis.
[d] Immunologically tolerant transgenic splenocytes.
[e] Unmanipulated.

the promotion stages may be reflected by the numbers and sizes of tumors, respectively. In the current study, the transfer of the $CD4^+$ and $CD8^+$ T-cell subsets caused differences not in the numbers or sizes but in the incidences of HCC, suggesting that the pathogenetic events directly affected neither stage of carcinogenesis. We speculate that the events induced by the individual subsets might be involved in triggering carcinogenetic environment to different extents in the earlier stage than in the initiation. And, irrespective of the causative T-cell subsets, initiation and promotion of HCC would occur when such environment was generated. This sequence of events suggests that the regulation of T cell-induced environment in the early period of hepatocarcinogenesis may inhibit tumor cell initiation and cancel

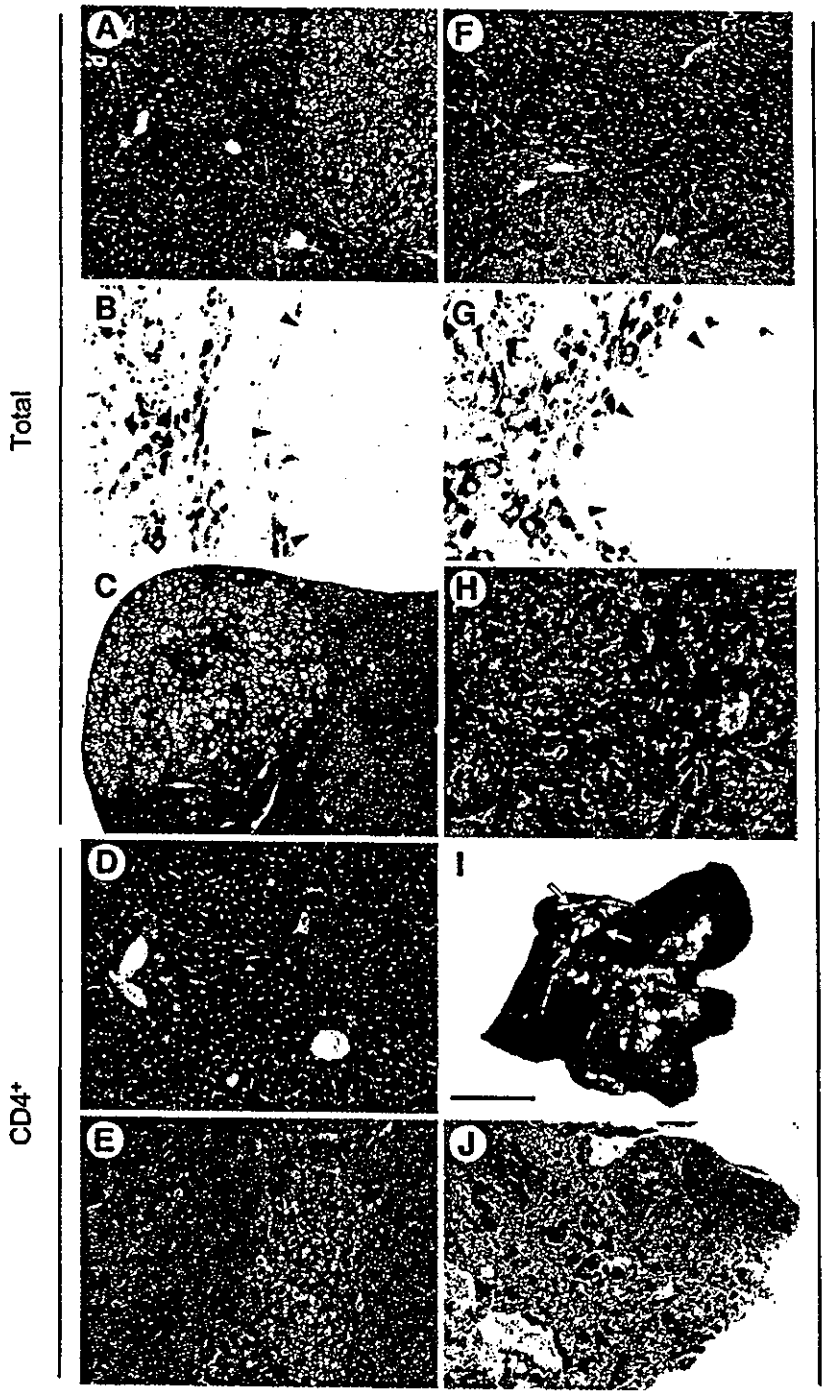

Fig. 5. Histopathological features of progressive liver disease and hepatocellular carcinomas (HCC) development after transfer of total (*A–C*), $CD4^+$ T cell-enriched (*D* and *E*) or $CD8^+$ T cell-enriched (*F–J*) splenocytes in a transgenic mouse model of chronic hepatitis B. The mice described in the legend to Fig. 2 were killed >11 months after the transfer, and liver tissues were stained with H&E (*A, C–F, H,* and *J*) and for hepatitis B surface antigen (HBsAg; *B* and *G*). Tumors in mice transferred with total splenocytes display histological evidence of well-differentiated HCC (*arrowheads; A*). The surrounding hepatic parenchyma show focal lobular inflammatory infiltrates associated with degenerating hepatocytes and marked lobular disarray. HBsAg expression is abolished in the tumor cells (*arrowheads*), whereas it is detectable in the surrounding parenchyma (*B*). In the same liver tissue as in *A*, well-differentiated HCC is seen that consists of tumor cells with large amounts of fatty deposits (*arrowheads; C*). Animals that received $CD4^+$-enriched cells demonstrate lower levels of inflammatory infiltrates (*D*) and clear tumor cell nests (*arrowheads; E*). Comparable with the mice that received total splenocyte transfer, animals that received $CD8^+$-enriched cells show well-differentiated HCC including clear cells (*arrowheads; F*), the histological features of chronic liver disease in the surrounding hepatic parenchyma, and the suppression of HBsAg expression in the tumor cells (*arrowheads; G*). In tumor tissues, both highly differentiated, fat-deposited neoplastic hepatocytes (*arrow; H, right area*) and sarcomatous component (*H, left area*) were seen. Furthermore, the mice were complicated with the rupture of HCC (*arrows; I* and *J*). Original magnifications: ×100 (*A, D, E, F,* and *J*), ×40 (*C*), and ×200 (*B, G,* and *H*). The *bar* represents 10 mm (*I*).

the following malignant transformation leading to tumor development.

The precise mechanisms of hepatocarcinogenesis during chronic viral hepatitis still remain unanswered. Within the entire spectrum of carcinogenic pathways including hepatic cell injury (13, 44, 45), proliferation (46–48), altered gene expression (49, 50), and the role of p53 (51–54), the current study design evaluating the late events in the carcinogenic process may not be sufficient to discuss the disease hypothesis. However, it is most likely, based on the striking similarity of the disease processes in human viral hepatitis and the animal model used in the current study (21, 22), that the T-cell subsets are critically involved in the pathogenesis of HCC associated with chronic hepatitis B. Elucidating the contribution of immunological events to the HCC development should be important not only for understanding the pathogenesis of liver cancer, but also for establishing new cancer-preventive treatments for patients with viral hepatitis.

ACKNOWLEDGMENTS

We thank Dr. Francis V. Chisari for kindly providing us the HBsAg transgenic mice, and Akemi Nakano, Yoko Hashimoto, Maki Kawamura, and Chiharu Minami for technical assistance.

REFERENCES

1. Di Bisceglie AM. Hepatitis C and hepatocellular carcinoma. Hepatology 1997;26: 34S–8S.
2. Ikeda K, Saitoh S, Suzuki Y, et al. Disease progression and hepatocellular carcinogenesis in patients with chronic viral hepatitis: a prospective observation of 2215 patients. J Hepatol 1998;28:930–8.

3. Kim CM, Koike K, Saito I, Miyamura T, Jay G. HBx gene of hepatitis B virus induces liver cancer in transgenic mice. Nature 1991;351:317–20.
4. Koike K, Moriya K, Iino S, et al. High-level expression of hepatitis B virus HBx gene and hepatocarcinogenesis in transgenic mice. Hepatology 1994;19:810–9.
5. Moriya K, Fujie H, Shintani Y, et al. The core protein of hepatitis C virus induces hepatocellular carcinoma in transgenic mice. Nat Med 1998;4:1065–7.
6. Lerat H, Honda M, Beard MR, et al. Steatosis and liver cancer in transgenic mice expressing the structural and nonstructural proteins of hepatitis C virus. Gastroenterology 2002;122:352–65.
7. Matsubara K, Tokino T. Integration of hepatitis B virus DNA and its implications for hepatocarcinogenesis. Mol Biol Med 1990;7:243–60.
8. Hildt E, Saher G, Bruss V, Hofschneider PH. The hepatitis B virus large surface protein (LHBs) is a transcriptional activator. Virology 1996;225:235–9.
9. Meyer M, Caselmann WH, Schluter V, Schreck R, Hofschneider PH, Baeuerle PA. Hepatitis B virus transactivator MHBst: activation of NF-kappa B, selective inhibition by antioxidants and integral membrane localization. EMBO J 1992;11:2991–3001.
10. Chisari FV, Klopchin K, Moriyama T, et al. Molecular pathogenesis of hepatocellular carcinoma in hepatitis B virus transgenic mice. Cell 1989;59:1145–56.
11. Dunsford HA, Sell S, Chisari FV. Hepatocarcinogenesis due to chronic liver cell injury in hepatitis B virus transgenic mice. Cancer Res 1990;50:3400–7.
12. Hagen TM, Huang S, Curnutte J, et al. Extensive oxidative DNA damage in hepatocytes of transgenic mice with chronic active hepatitis destined to develop hepatocellular carcinoma. Proc Natl Acad Sci USA 1994;91:12808–12.
13. Chisari FV, Ferrari C. Hepatitis B virus immunopathogenesis. Annu Rev Immunol 1995;13:29–60.
14. Cerny A, Chisari FV. Immunological aspects of HCV infection. Intervirology 1994; 37:119–25.
15. Chang KM, Rehermann B, Chisari FV. Immunopathology of hepatitis C. Springer Semin. Immunopathol 1997;19:57–68.
16. Rehermann B, Chisari FV. Cell mediated immune response to the hepatitis C virus. Curr Top Microbiol Immunol 2000;242:299–325.
17. Moriyama T, Guilhot S, Klopchin K, et al. Immunobiology and pathogenesis of hepatocellular injury in hepatitis B virus transgenic mice. Science 1990;248:361–4.
18. Ando K, Moriyama T, Guidotti LG, et al. Mechanisms of class I restricted immunopathology. A transgenic mouse model of fulminant hepatitis. J Exp Med 1993;178: 1541–54.
19. Ando K, Guidotti LG, Wirth S, et al. Class I-restricted cytotoxic T lymphocytes are directly cytopathic for their target cells in vivo. J Immunol 1994;152:3245–53.
20. Franco A, Guidotti LG, Hobbs MV, Pasquetto V, Chisari FV. Pathogenetic effector function of CD4-positive T helper 1 cells in hepatitis B virus transgenic mice. J Immunol 1997;159:2001–8.
21. Nakamoto Y, Guidotti LG, Kuhlen CV, Fowler P, Chisari FV. Immune pathogenesis of hepatocellular carcinoma. J Exp Med 1998;188:341–50.
22. Nakamoto Y, Kaneko S, Fan H, et al. Prevention of hepatocellular carcinoma development associated with chronic hepatitis by anti-fas ligand antibody therapy. J Exp Med 2002;196:1105–11.
23. Kondo T, Suda T, Fukuyama H, Adachi M, Nagata S. Essential roles of the Fas ligand in the development of hepatitis. Nat Med 1997;3:409–13.
24. Nakamoto Y, Guidotti LG, Pasquetto V, Schreiber RD, Chisari FV. Differential target cell sensitivity to CTL-activated death pathways in hepatitis B virus transgenic mice. J Immunol 1997;158:5692–7.
25. Suda T, Takahashi T, Golstein P, Nagata S. Molecular cloning and expression of the Fas ligand, a novel member of the tumor necrosis factor family. Cell 1993;75: 1169–78.
26. Rouvier E, Luciani MF, Golstein P. Fas involvement in Ca(2+)-independent T cell-mediated cytotoxicity. J Exp Med 1993;177:195–200.
27. Anel A, Buferne M, Boyer C, Schmitt-Verhulst AM, Golstein P. T cell receptor-induced Fas ligand expression in cytotoxic T lymphocyte clones is blocked by protein tyrosine kinase inhibitors and cyclosporin A. Eur J Immunol 1994;24:2469–76.
28. Vignaux F, Vivier E, Malissen B, Depraetere V, Nagata S, Golstein P. TCR/CD3 coupling to Fas-based cytotoxicity. J Exp Med 1995;181:781–6.
29. Suda T, Okazaki T, Naito Y, et al. Expression of the Fas ligand in cells of T cell lineage. J Immunol 1995;154:3806–13.
30. Chisari FV, Filippi P, McLachlan A, et al. Expression of hepatitis B virus large envelope polypeptide inhibits hepatitis B surface antigen secretion in transgenic mice. J Virol 1986;60:880–7.
31. Chisari FV, Filippi P, Buras J, et al. Structural and pathological effects of synthesis of hepatitis B virus large envelope polypeptide in transgenic mice. Proc Natl Acad Sci USA 1987;84:6909–13.
32. Wirth S, Guidotti LG, Ando K, Schlicht HJ, Chisari FV. Breaking tolerance leads to autoantibody production but not autoimmune liver disease in hepatitis B virus envelope transgenic mice. J Immunol 1995;154:2504–15.
33. Coligan JE, Kruisbeek AM, Margulies DH, Shevach EM, Strober W. Current Protocols in Immunology. New York: John Wiley & Sons, Inc., 1994.
34. Guidotti LG, Martinez V, Loh YT, Rogler CE, Chisari FV. Hepatitis B virus nucleocapsid particles do not cross the hepatocyte nuclear membrane in transgenic mice. J Virol 1994;68:5469–75.
35. Urase K, Fujita E, Miho Y, et al. Detection of activated caspase-3 (CPP32) in the vertebrate nervous system during development by a cleavage site-directed antiserum. Brain Res Dev Brain Res 1998;111:77–87.
36. Guidotti LG, Ishikawa T, Hobbs MV, Matzke B, Schreiber R, Chisari FV. Intracellular inactivation of the hepatitis B virus by cytotoxic T lymphocytes. Immunity 1996;4:25–36.
37. Guidotti LG, Rochford R, Chung J, Shapiro M, Purcell R, Chisari FV. Viral clearance without destruction of infected cells during acute HBV infection. Science 1999;284: 825–9.
38. Gilles PN, Guerrette DL, Ulevitch RJ, Schreiber RD, Chisari FV. HBsAg retention sensitizes the hepatocyte to injury by physiological concentrations of interferon-gamma. Hepatology 1992;16:655–63.
39. Homann D, Teyton L, Oldstone MB. Differential regulation of antiviral T-cell immunity results in stable CD8+ but declining CD4+ T-cell memory. Nat Med 2001;7:913–9.
40. Lau LL, Jamieson BD, Somasundaram T, Ahmed R. Cytotoxic T-cell memory without antigen. Nature 1994;369:648–52.
41. Murali-Krishna K, Lau LL, Sambhara S, Lemonnier F, Altman J, Ahmed R. Persistence of memory CD8 T cells in MHC class I-deficient mice. Science 1999;286: 1377–81.
42. Kaech SM, Wherry EJ, Ahmed R. Effector and memory T-cell differentiation: implications for vaccine development. Nat Rev Immunol 2002;2:251–62.
43. Perez-Losada J, Balmain A. Stem-cell hierarchy in skin cancer. Nat Rev Cancer 2003;3:434–43.
44. Liang TJ, Rehermann B, Seeff LB, Hoofnagle JH. Pathogenesis, natural history, treatment, and prevention of hepatitis C. Ann Intern Med 2000;132:296–305.
45. Nakamoto Y, Kaneko S. Mechanisms of viral hepatitis induced liver injury. Curr Mol Med 2003;3:537–44.
46. Columbano A, Shinozuka H. Liver regeneration versus direct hyperplasia. FASEB J 1996;10:1118–28.
47. Sell S. Heterogeneity and plasticity of hepatocyte lineage cells. Hepatology 2001;33: 738–50.
48. Coleman WB. Mechanisms of human hepatocarcinogenesis. Curr Mol Med 2003;3: 573–88.
49. Shirota Y, Kaneko S, Honda M, Kawai HF, Kobayashi K. Identification of differentially expressed genes in hepatocellular carcinoma with cDNA microarrays. Hepatology 2001;33:832–40.
50. Xu XR, Huang J, Xu ZG, et al. Insight into hepatocellular carcinogenesis at transcriptome level by comparing gene expression profiles of hepatocellular carcinoma with those of corresponding noncancerous liver. Proc Natl Acad Sci USA 2001;98: 15089–94.
51. Hsu IC, Metcalf RA, Sun T, Welsh JA, Wang NJ, Harris CC. Mutational hotspot in the p53 gene in human hepatocellular carcinomas. Nature 1991;350:427–8.
52. Bressac B, Kew M, Wands J, Ozturk M. Selective G to T mutations of p53 gene in hepatocellular carcinoma from southern Africa. Nature 1991;350:429–31.
53. Kern MA, Breuhahn K, Schirmacher P. Molecular pathogenesis of human hepatocellular carcinoma. Adv Cancer Res 2002;86:67–112.
54. Eferl R, Ricci R, Kenner L, et al. Liver tumor development. c-Jun antagonizes the proapoptotic activity of p53. Cell 2003;112:181–92.

JOURNAL OF VIROLOGY, Mar. 2004, p. 2738–2748 Vol. 78, No. 6
0022-538X/04/$08.00+0 DOI: 10.1128/JVI.78.6.2738–2748.2004

Effect of Interaction between Hepatitis C Virus NS5A and NS5B on Hepatitis C Virus RNA Replication with the Hepatitis C Virus Replicon

Tetsuro Shimakami,[1,2] Makoto Hijikata,[3] Hong Luo,[1,4] Yuan Yuan Ma,[1] Shuichi Kaneko,[2] Kunitada Shimotohno,[3] and Seishi Murakami[1]*

Department of Molecular Oncology, Cancer Research Institute, Kanazawa University,[1] and Department of Gastroenterology, Kanazawa University Graduate School of Medicine,[2] Takara-Machi, Kanazawa, Ishikawa 920-0934, and Department of Viral Oncology, Institute for Virus Research, Kyoto University, Sakyo-Ku, Kyoto 606-8507,[3] Japan, and The Institute of Infectious Diseases, West China Hospital, Sichuan University, Chengdu, Sichuan 610041, China[4]

Received 3 September 2003/Accepted 10 November 2003

Hepatitis C virus (HCV) NS5A has been reported to be important for the establishment of replication by adaptive mutations or localization, although its role in viral replication remains unclear. It was previously reported that NS5A interacts with NS5B via two regions of NS5A in the isolate JK-1 and modulates the activity of NS5B RdRp (Y. Shirota et al., J. Biol. Chem., 277:11149–11155, 2002), but the biological significance of this interaction has not been determined. In this study, we addressed the effect of this interaction on HCV RNA replication with an HCV replicon system derived from the isolate M1LE (H. Kishine et al., Biochem. Biophys. Res. Commun., 293:993–999, 2002). We constructed three internal deletion mutants, M1LE/5Adel-1 and M1LE/5Adel-2, each encoding NS5A which cannot bind NS5B, and M1LE/5Adel-3, encoding NS5A that can bind NS5B. After transfection into Huh-7 cells, M1LE/5Adel-3 was replication competent, but both M1LE/5Adel-1 and M1LE/5Adel-2 were not. Next we prepared 20 alanine-substituted clustered mutants within both NS5B-binding regions and examined the effect of these mutants on HCV RNA replication. Only 5 of the 20 mutants were replication competent. Subsequently, we introduced a point mutation, S225P, a deletion of S229, or S232I into NS5A and prepared cured Huh-7 cells that were cured of RNA replication by alpha interferon. Finally, with these point mutations and cured cells, we established a highly improved replicon system. In this system, only the same five mutants were replication competent. These results strongly suggest that the interaction between NS5A and NS5B is critical for HCV RNA replication in the HCV replicon system.

The hepatitis C virus (HCV) is a major cause of chronic hepatitis around the world (1, 9). Chronic infection with HCV results in liver cirrhosis and often hepatocellular carcinoma (50, 53). HCV is an enveloped positive-strand RNA virus belonging to the genus *Hepacivirus* in the family *Flaviviridae* (44). The HCV RNA genome is ~9.6 kb in length and consists of a 5′ nontranslated region (5′ NTR), a large open reading frame, and a 3′ NTR. The 5′ NTR contains an internal ribosome entry site (IRES) mediating translation of a single polyprotein of ~3,000 amino acid (aa) residues (57, 59). The polyprotein is cleaved by host and viral protease into at least 10 different products (2, 21, 22, 25, 26). The structural proteins core, E1, and E2 are located in the amino terminus of the polyprotein, followed by p7, a hydrophobic peptide with unknown function, and the nonstructural (NS) proteins NS2, NS3, NS4A, NS4B, NS5A, and NS5B (41). The 3′ NTR consists of a short variable sequence, a poly(U)-poly(UC) tract, and a highly conserved X region, and it is critical for HCV RNA replication and HCV infection (17, 34, 65, 66).

HCV is unique among positive-strand RNA viruses in causing persistent infections, and a high mutation rate in E2 allows it to escape host immune surveillance. These phenomena are tightly associated with chronic inflammation of the liver (27, 32, 61, 62). Therefore, HCV RNA replication has been a target for treatment of HCV. NS5B is an RNA-dependent RNA polymerase (RdRp), the central catalytic enzyme in HCV RNA replication. Several recombinant forms of NS5B expressed and purified from insect cells and *Escherichia coli* are available and catalytically active, and studies with purified NS5B proteins provide insight into the biochemical and catalytic properties of NS5B (3, 16, 39, 64). However, the result that NS5B can initiate de novo RNA replication in vitro with both a non-HCV RNA template and an HCV RNA template may reflect the catalytic property of NS5B but not the tight regulation of HCV RNA replication initiation. Studies of HCV RNA replication in vitro have to overcome several difficulties, since replication requires all or most NS proteins and occurs at the membrane where all of the HCV NS proteins are recruited.

A second system used to study HCV RNA replication is the study of HCV RNA replicons in vivo, which utilizes autonomously replicating HCV-derived RNAs. These replicon RNAs have the authentic HCV 5′ and 3′ NTRs. The HCV IRES drives the translation of a selectable marker such as neomycin resistance, and an internal encephalomyocarditis virus IRES directs translation of NS3 to NS5B (38). In vitro-transcribed replicon RNAs are transfected into the human hepatoma cell line Huh-7 by electroporation and placed under selection. The emergence of neomycin-resistant cell colonies is indicative of

* Corresponding author. Mailing address: Department of Molecular Oncology, Cancer Research Institute, Kanazawa University, 13-1 Takara-Machi, Kanazawa, 920-0934 Ishikawa, Japan. Phone: 81-76-265-2731. Fax: 81-76-234-4501. E-mail: semuraka@kenroku.kanazawa-u.ac.jp.

RNA replication. Recently, adaptive mutations that dramatically enhance the ability of HCV RNA to replicate have been identified in NS3, NS4B, NS5A, and NS5B (4, 24, 35, 37, 40). Initially, only the replicon derived from a genotype 1b isolate, HCV-Con1, was replication competent in Huh-7 cells, and adaptive mutations were required for efficient replication (4, 35, 37, 40). Then, several replicon systems derived from a genotype 1b isolate, HCV-N, and a genotype 1a isolate, HCV-H77, were reported to replicate in Huh-7 cells (6, 23, 24, 29). Recently, a replicon system was established which uses an HCV sequence derived from the human T-cell line MT-2C infected with HCV (a genotype 1b isolate, M1LE) in vitro and isolated 50-1 cells replicating subgenomic RNAs with some amino acid mutations (31, 33, 43, 55).

It was previously reported that NS5A and NS5B interact in vitro and in vivo through two independent regions of NS5A and that NS5A modulates the activity of NS5B RdRp through this interaction in vitro in the isolate JK-1 (54). This ability of NS5A to modulate the RdRp activity in vitro may be consistent with the high frequency of adaptive mutations in NS5A which result in a much more efficient RNA replication in Huh-7 cells; however, the biological meaning of the interaction between NS5A and NS5B remains to be addressed in vivo. Here we report a modified HCV RNA replicon system derived from the isolate M1LE by introducing point mutations (S225P, a deletion of S229, and S2321), and curing 50-1 cells of HCV subgenomic RNA replication by interferon (IFN) treatment. By introducing internal deletion and substitution mutations into NS5A, we demonstrate that the regions essential for the interaction between NS5A and NS5B are also critical for HCV RNA replication in using the HCV replicon system.

MATERIALS AND METHODS

Construction of plasmids. pNNRZ2RU (33) harbors a subgenomic replicon derived from MT-2C cells infected with HCV (a genotype 1b isolate, M1LE; GenBank accession no. AB080299), and this plasmid contains cDNA of wild-type M1LE. For convenience, pNNRZ2RU was digested with *Mlu*I and *Bgl*II, and the obtained fragment was inserted into the *Mlu*I and *Bgl*II sites of the vector pGL3Basic (Promega) to create pGL3-*Mlu*I-*Bgl*II. pGL3-*Mlu*I-*Bgl*II was used as an intermediate vector. All mutations were introduced into pGL3-*Mlu*I-*Bgl*II, and then the fragments of pGL3-*Mlu*I-*Bgl*II digested by *Mlu*I and *Bgl*II containing each mutation were reintroduced into the *Mlu*I and *Bgl*II sites of pNNRZ2RU to create each mutant.

M1LE/5Adel-1 was generated by PCR with the primers 5Adel-1 For (containing a *Mlu*I site) and 5A Rev-3 and then inserted into the *Mlu*I and *Nhe*I sites of pGL3-*Mlu*I-*Bgl*II to create pGL3-*Mlu*I-*Bgl*II-5Adel-1. M1LE/5Adel-2 was generated by PCR with overlap extension with the primers 5Adel-2 For, 5A Rev-2, 5Adel-2 Rev, and 5A For-3 and then inserted into the *Nhe*I and *Sac*I sites of pGL3-*Mlu*I-*Bgl*II to create pGL3-*Mlu*I-*Bgl*II-5Adel-2. M1LE/5Adel-3 was generated by PCR with the primers 5A del-3 For (containing a *Nhe*I site) and 5A Rev-2 and then inserted into the *Nhe*I and *Sac*I sites of pGL3-*Mlu*I-*Bgl*II to create pGL3-*Mlu*I-*Bgl*II-5Adel-3.

An alanine scanning method was used to construct NS5A alanine-substituted mutants to minimize the effects of substituted amino acid residues (7). The positions of alanine-substituted clustered mutations (cm) of NS5A are shown in Fig. 2B. To generate M1LE/cm 94, 100, 105, 110, 113, 120, 127, 134, 141, 148, and 155, each mutation was introduced into the *Mlu*I and *Nhe*I sites of pGL3-*Mlu*I-*Bgl*II by site-directed mutagenesis with primers carrying the necessary nucleotide changes to create pGL3-*Mlu*I-*Bgl*II-cm94, -100, -105, -110, -113, -120, -127, -134, -141, -148, and -155, respectively. To generate M1LE/cm 252, 277, 283, 290, 297, 304, 311, 316, 321, and 328, each mutation was introduced into the *Nhe*I and *Sac*I sites of pGL3-*Mlu*I-*Bgl*II by site-directed mutagenesis with primers carrying the necessary nucleotide changes to create pGL3-*Mlu*I-*Bgl*II-cm252, -277, -283, -290, -297, -304, -311, -316, -321, and -328, respectively.

To generate M1LE/S225P and a deletion of S229 (delS229), the point mutations S225P and delS229 were introduced into the *Mlu*I and *Nhe*I sites of pGL3-*Mlu*I-*Bgl*II by site-directed mutagenesis with primers carrying the necessary nucleotide changes to create pGL3-*Mlu*I-*Bgl*II-S225P and -delS229. The point mutation S2321 was introduced into the *Mlu*I and *Sac*I sites of pGL3-*Mlu*I-*Bgl*II by site-directed mutagenesis with primers carrying the necessary nucleotide changes to create pGL3-*Mlu*I-*Bgl*II-S2321. To generate the double mutants containing both the point mutation S2321 plus an internal deletion mutation or cm, the *Eco*RI fragments of pGL3-*Mlu*I-*Bgl*II-cm94, -100, -105, -110, -113, -120, -127, -134, and -141 were inserted into the *Eco*RI sites of pGL3-*Mlu*I-*Bgl*II-S2321. Because there were no optimal enzyme sites in the others, the point mutation S2321 was introduced into the *Mlu*I and *Sac*I sites of pGL3-*Mlu*I-*Bgl*II-5Adel-1, -del-2, -del-3, and -cm148, -155, -252, -277, -283, -290, -297, -304, -311, -316, -321, and -328 by site-directed mutagenesis with primers carrying the necessary nucleotide changes.

To create double mutants containing both the point mutation S225P plus an internal deletion mutation or cm (cm 252, 277, 283, 290, 297, 304, 311, 316, 321, and 328), the *Nhe*I and *Sac*I fragments of pGL3-*Mlu*I-*Bgl*II-5Adel-2, -5Adel-3, -cm252, -277, -283, -290, -297, -304, -311, -316, -321, and -328 were introduced into the *Nhe*I and *Sac*I sites of pGL3-*Mlu*I-*Bgl*II-S225P.

To generate M1LE/5B-VDD, a point mutation changing the GDD motif of NS5B to VDD was introduced at the *Nde*I and *Sma*I sites of pGL3-*Mlu*I-*Bgl*II by site-directed mutagenesis with primers carrying the necessary nucleotide changes to create pGL3-*Mlu*I-*Bgl*II-5B-VDD.

All of the mammalian expression vectors were derived from pSG5UTPL (36). The vector pNKFLAG (49) was used to express amino-terminally FLAG-tagged proteins. The vector pNKGST (49) was used to express glutathione *S*-transferase (GST)-fused proteins.

pNNRZ2RU was subcloned by PCR with the primers NS5A For, NS5A Rev, NS5B For, and NS5B Rev. NS5A For contains an artificial initiation codon downstream of the *Mun*I site, and NS5B For contains one artificial initiation codon downstream of the *Sac*I site. NS5A Rev contains a *Bgl*II site, and NS5B Rev contains a *Bam*HI site. Full-length NS5A was subcloned into the *Eco*RI and *Bam*HI sites of pNKFLAG to create pNKFLAG-5A/wild, and full-length NS5B was subcloned into the *Sac*I and *Bam*HI sites of pNKGST to create pNKGST-5B/wild.

To create NKFLAG-5A/del-1, and -cm94, -100, -105, -113, -120, -127, -134, -141, -148, and -155, the *Mlu*I and *Nhe*I fragments of pGL3-*Mlu*I-*Bgl*II mutants were introduced at the *Mlu*I and *Nhe*I sites of pNKFLAG-5A/wild. To create NKFLAG-5A/del-2, /del-3, -cm252, -277, -283, -290, -297, -304, -311, -316, -321, and -328, the *Nhe*I and *Sac*I fragments of pGL3-*Mlu*I-*Bgl*II mutants were inserted into the *Nhe*I and *Sac*I sites of pNKFLAG-5A/wild.

The sequences of all of the constructs were confirmed by the dideoxy sequence method. The main primers used for plasmid construction are shown in Table 1.

In vitro transcription and purification of RNA. Plasmids were linearized with *Xba*I and purified by passage through a column (PCR purification kit; Qiagen) prior to transcription. RNA was synthesized with T7 MEGAScript reagents (Ambion) by following the manufacturer's directions, and the reaction was stopped by digestion with RNase-free DNase. The synthesized RNA was passed

TABLE 1. Sequences of primers used in the present study

Primer	Sequence (5′–3′)
5Adel-1 For	ATATATCAACGCGTACCCGGCGTGTAAACCTCTCCTACGG
5Adel-2 For	GTGGAGTCAGAGAACGTTCCTCCGGTGGTACACGGGTGCCCA
5Adel-2 Rev	TACCACCGGAGGAACGTTCTCTGACTCCACGCGGGTGATGTT
5Adel-3 For	ATATATATGCTAGCCAGTTGAAGGTAGTAATTCTGGACTCTTTC
5A For-3	ATCCTTCCCACATTACAGCA
5A Rev-2	CTCAACGTCGGATCCCTTGT
5A Rev-3	GGTCAGCGTCCGGGGAGTCATG
NS5A For	ATATCAATTGCATGTCCGGCTCGTGGCTAAGGGATATT
NS5A Rev	ATATAGATCTGCAGCAGACGACGTCCTCACTAGCCTC
NS5B For	TATCGAGCTCGATGTCAATGTCCTACTCATGGACAGGT
NS5B Rev	ATATGGGATCCCCGGTTGGGGAGCAGGTAGATGCCTAC